Abnormal Synaptic Vesicle Biogenesis in Drosophila Synaptogyrin Mutants

Citation: Stevens, R. J., Y. Akbergenova, R. A. Jorquera, and J. T. Littleton. "Abnormal Synaptic Vesicle Biogenesis in Drosophila Synaptogyrin Mutants." Journal of Neuroscience 32, no. 50 (December 12, 2012): 18054-18067.

As Published: http://dx.doi.org/10.1523/jneurosci.2668-12.2012

Publisher: Society for Neuroscience

Persistent URL: http://hdl.handle.net/1721.1/79760

Version: Final published version: final published article, as it appeared in a journal, conference proceedings, or other formally published context

Cellular/Molecular

Abnormal Synaptic Vesicle Biogenesis in *Drosophila Synaptogyrin* Mutants

Robin J. Stevens, Yulia Akbergenova, Ramon A. Jorquera, and J. Troy Littleton

The Picower Institute for Learning and Memory, Department of Biology, Department of Brain and Cognitive Sciences, Massachusetts Institute of Technology, Cambridge, Massachusetts 02139

Sustained neuronal communication relies on the coordinated activity of multiple proteins that regulate synaptic vesicle biogenesis and cycling within the presynaptic terminal. Synaptogyrin and synaptophysin are conserved MARVEL domain-containing transmembrane proteins that are among the most abundant synaptic vesicle constituents, although their role in the synaptic vesicle cycle has remained elusive. To further investigate the function of these proteins, we generated and characterized a *synaptogyrin* (*gyr*)-null mutant in *Drosophila*, whose genome encodes a single synaptogyrin isoform and lacks a synaptophysin homolog. We demonstrate that *Drosophila* synaptogyrin plays a modulatory role in synaptic vesicle biogenesis at larval neuromuscular junctions. *Drosophila* lacking synaptogyrin are viable and fertile and have no overt deficits in motor function. However, ultrastructural analysis of *gyr* larvae revealed increased synaptic vesicle diameter and enhanced variability in the size of synaptic vesicles. In addition, the resolution of endocytic cisternae into synaptic vesicles in response to strong stimulation is defective in *gyr* mutants. Electrophysiological analysis demonstrated an increase in quantal size and a concomitant decrease in quantal content, suggesting functional consequences for transmission caused by the loss of synaptogyrin. Furthermore, high-frequency stimulation resulted in increased facilitation and a delay in recovery from synaptic depression, indicating that synaptic vesicle exo-endocytosis is abnormally regulated during intense stimulation conditions. These results suggest that synaptogyrin modulates the synaptic vesicle exo-endocytic cycle and is required for the proper biogenesis of synaptic vesicles at nerve terminals.

Introduction

Synaptogyrin and synaptophysin are evolutionarily related members of the MARVEL domain family, which defines a group of tetraspanning membrane proteins involved in vesicle trafficking and membrane apposition events (Hübner et al., 2002; Sánchez-Pulido et al., 2002). The two proteins are abundantly expressed on synaptic vesicles, with synaptophysin alone constituting ~10% of synaptic vesicle protein by mass in rats (Takamori et al., 2006). Synaptophysin can oligomerize into homomultimers and has been proposed to form an ion channel or proteinaceous fusion pore (Rehm et al., 1986; Thomas et al., 1988; Gincel and Shoshan-Barmatz, 2002; Arthur and Stowell, 2007). Synaptophysin also has been implicated in regulating synaptic vesicle exocytosis, perhaps via its interaction with synaptobrevin/VAMP2, which precludes the association of synaptobrevin with other members of the SNARE complex (Edelmann et al., 1995).

Synaptophysin and synaptogyrin family members may also play a role in shaping lipid membranes and promoting vesicle biogenesis. Synaptophysin binds cholesterol and promotes the formation of highly curved membranes (Thiele et al., 2000). Overexpression of cellugyrin, a non-neuronal paralog of synaptogyrin, induces the formation of synaptic-like microvesicles in neuroendocrine cells (Belfort et al., 2005). Synaptophysin may also participate in synaptic vesicle recycling through a Ca^{2+}-dependent interaction with dynamin, as the inhibition of this interaction results in a smaller synaptic vesicle pool following high-frequency stimulation (Daly et al., 2000; Daly and Ziff, 2002). Similarly, a recent study demonstrated the kinetics of endocytosis is slowed in cultured neurons during periods of sustained stimulation in the absence of synaptophysin (Kwon and Chapman, 2011).

Although synaptophysin and synaptogyrin are evolutionarily conserved and abundant in neurons, the loss of these proteins results in relatively mild phenotypes. Initial characterization of a *Caenorhabditis elegans* triple knock-out of synaptophysin, synaptogyrin, and the tetraspanning membrane protein SCAMP revealed no detectable phenotypes in addition to a slight increase in clathrin-coated synaptic vesicles (Abraham et al., 2006). Closer examination of the *C. elegans synaptogyrin* mutant identified slightly altered motility and changes in sensitivity to drugs affecting GABAergic and cholinergic signaling (Abraham et al., 2011). Similarly, *synaptophysin* knock-out mice, while viable and fertile, have mild defects, including altered synaptic vesicle density and morphology in photoreceptors that lack the synaptophysin paralog synaptoporin (McMahon et al., 1996; Spiwoks-Becker et al., 2001). Synaptophysin/synaptogyrin double knock-out mice also display defects in paired-pulse facilita-

Received June 4, 2012; revised Oct. 11, 2012; accepted Oct. 28, 2012.

Author contributions: R.J.S., Y.A., R.A.J., and J.T.L. designed research; R.J.S., Y.A., and R.A.J. performed research; R.J.S., Y.A., R.A.J., and J.T.L. analyzed data; R.J.S. and J.T.L. wrote the paper.

This work was supported by National Institutes of Health Grant NS40296 (J.T.L.). R.A.J. was a recipient of the PEW Latin American Fellows Program in the Biomedical Sciences.

The authors declare no competing financial interests.

Correspondence should be addressed to J. Troy Littleton, The Picower Institute for Learning and Memory, Massachusetts Institute of Technology, 43 Vassar Street, 46-3243, Cambridge, MA 02139. E-mail: troy@mit.edu.

R.A. Jorquera's present address: Neuroscience Department, Universidad Central del Caribe, Bayamon, Puerto Rico, 00960-6032.

DOI:10.1523/JNEUROSCI.2668-12.2012

 0270-6474/12/3218054-14$15.00/0

tion, post-tetanic potentiation, and long-term potentiation (Janz et al., 1999).

The genetic analysis of synaptophysin and synaptogyrin in mice is complicated by the presence of multiple homologs with some degree of functional redundancy (Janz et al., 1999; Spiwoks-Becker et al., 2001). We therefore sought to investigate synaptogyrin function in *Drosophila*, which lacks a synaptophysin homolog and has only one synaptogyrin family member. The loss of synaptogyrin in *Drosophila* leads to changes in synaptic vesicle size and delays in resolving endocytic cisternae, as well as alterations in quantal size and evoked release during high-frequency stimulation.

Materials and Methods

Homology searches and protein alignment. NCBI BLAST (blastp) was used to identify potential homologs, which were confirmed using a reciprocal blastp search (http://blast.ncbi.nlm.nih.gov). TMHMM Server v. 2.0 (http://www.cbs.dtu.dk/services/TMHMM) was used to verify prospective homologs had four transmembrane domains in the correct orientation (cytoplasmic N and C termini). The synaptogyrin protein alignment was generated using the T-Coffee algorithm (http://tcoffee.org) with default settings (Notredame et al., 2000; Di Tommaso et al., 2011). CLC DNA Workbench 4.0 was used to visualize the alignment. Synaptogyrin GenBank accession numbers used for Figure 1: *Drosophila melanogaster*, AAF58329; *Homo sapiens*, EAW60323 (isoform 1a); *Monosiga brevicollis*, EDQ85723.

Fly stocks and transgenics. Flies were cultured using standard media and techniques at room temperature (~22°C) unless otherwise noted. The GAL4/UAS system was used to drive neuronal expression of selected transgenes using the driver *elav^{c155}-GAL4* (Brand and Perrimon, 1993). The UAS-synaptogyrin-GFP (gyrin-GFP) line was generated by subcloning full-length *Drosophila* synaptogyrin cDNA (minus the stop codon) into a pUAST vector containing a C-terminal GFP tag. This construct was then injected into *w^{1118}* embryos at Duke University Model Systems Genomics (Durham, NC). The UAS-myc-synaptogyrin construct used for rescue experiments was constructed by inserting full-length synaptogyrin cDNA into a modified pValum vector containing an N-terminal myc tag (Cho et al., 2010). This construct was injected into a strain carrying the *attP2* site (*yv;;attP2*) for targeted transgene insertion on the third chromosome (Markstein et al., 2008; Ni et al., 2008) at Genetic Services.

Synaptogyrin antibody generation and Western blotting. The C-terminal fragment of *Drosophila* synaptogyrin (gyrin-cterm) encoding amino acids 181–241 was amplified from a *Drosophila* cDNA library and subcloned into the pGEX-4T-1 vector (GE Healthcare). Recombinant GST-gyrin-cterm was expressed and processed in *Escherichia coli* (BL21) using standard protocols. The fusion protein was purified from cell lysates using Glutathione Sepharose 4B (GE Healthcare) and used to immunize rabbits for polyclonal antibody production (Invitrogen). Western analysis was performed using standard protocols. Primary antibody dilutions were as follows: synaptogyrin, 1:20,000 and complexin, 1:5000 (Huntwork and Littleton, 2007). IRDye 800-conjugated goat anti-rabbit secondary antibodies were used at a dilution of 1:10,000 (LI-COR Biosciences). Western blots were visualized with an Odyssey infrared imaging system (LI-COR Biosciences).

Generation of a synaptogyrin-null mutant. Two independent deletions of the *synaptogyrin* locus were generated by imprecise excision of a P-element (P{lacW}l(2)SH0644^{SH0644}) located ~500 bp upstream of the synaptogyrin translation start site in the first exon of the gene. Two hundred *white*$^{-}$ excision events were screened by PCR and two resulted in deletions that extended into the *synaptogyrin* locus beyond the translation start site. A precise excision line isolated from the screen, *gyr^{PE}*, was confirmed by sequencing and used as a control for genetic background in all experiments. To confirm that the deletions in *gyr^{1}* and *gyr^{2}* did not generate truncated versions of synaptogyrin, Western blots were performed on protein extracts from these lines. The polyclonal antibody raised against the synaptogyrin protein targets the C terminus, and this coding region was left intact in both alleles. Synaptogyrin immunoreactivity was completely absent in *gyr^{1}* and *gyr^{2}* animals by Western blot, suggesting these represent null mutations. *gyr^{1}* and *gyr^{2}* are in the *white* (*w^{1118}*) background unless otherwise indicated.

Immunohistochemistry. Wandering third instar larvae were dissected in Ca^{2+}-free HL3.1 saline (70 mM NaCl, 5 mM KCl, 10 mM $NaHCO_3$, 4 mM $MgCl_2$, 5 mM trehalose, 115 mM sucrose, and 5 mM HEPES, pH 7.2) and fixed for 45 min in HL3.1 containing 4% formaldehyde. Fixations using the synaptogyrin antibody (α-Gyr) were performed for 5 min in ice-cold 100% methanol. Primary antibody dilutions were as follows: synaptogyrin, 1:500; Discs large (Dlg), 1:250; nc82/bruchpilot, 1:100; synaptotagmin 1, 1:200 (3H2 2D7, from K. Zinn). Secondary antibodies were used at a dilution of 1:250 and include Cy2-conjugated goat anti-rabbit, Cy3-conjugated goat anti-rabbit, Rhodamine Red-conjugated donkey anti-mouse (Jackson ImmunoResearch), and Alexa Fluor 488-conjugated goat anti-mouse (Invitrogen). Goat α-horseradish peroxidase (HRP) antibodies conjugated to either fluorescein isothiocyanate or Rhodamine Red were added as secondary antibodies and were used at a concentration of 1:10,000 or 1:500, respectively. Images were acquired with an Axoplan 2 confocal microscope using PASCAL software (Carl Zeiss MicroImaging).

Bouton and active zone counting. Age-matched wandering third instar larvae were grown at low density at 25°C and immunohistochemistry was performed as described above. Bouton quantification was performed using antibodies against HRP and Dlg. Active zone number was quantified using monoclonal nc82 antibodies, which recognize the active zone component bruchpilot (Wagh et al., 2006). To control for staining variability, larvae of different genotypes were processed together. All bouton and active zone measurements were quantified at muscle 6/7 of segment A3. Image analysis was performed using ImageJ software (National Institutes of Health; NIH). Bouton number is known to be proportional to muscle size (Lnenicka and Keshishian, 2000); however, since muscle area did not differ significantly between *gyr* and control larvae, no corrections were necessary. Bouton and active zone quantification were performed blind to genotype.

Electron microscopy. Dissected *Drosophila* third instar larvae were fixed for 1 h in 4% paraformaldehyde/1% glutaraldehyde in 0.1 M cacodylate buffer, pH 7.2. For the indicated experiments, preparations were stimulated before fixation with 90 mM high K^+ solution or with 10 consecutive stimulation trains at a frequency of 100 Hz. Each pulse was 1 s in duration and was followed by a 1 s rest period. Preparations were fixed immediately after stimulation. Fixed larvae were washed in standard HL3 solution for 1 h and postfixed for 40 min in 1% osmium tetroxide. Specimens were dehydrated in a graded series of ethanol and water mixtures up to 100% ethanol followed by acetone. Samples were pre-infiltrated for 1 h in a 1:1 mixture of acetone and Epon and then embedded in fresh Epon overnight at 60°C. Thin sections (60–70 nm) were contrasted with 0.2% lead citrate and imaged at 80 kV on an FEI Tecnai G2 Spirit transmission electron microscope (TEM) equipped with an AMT CCD camera. Imaging was performed at the W.M. Keck Microscopy Facility at the Whitehead Institute. Quantification of synaptic vesicle diameter and density was performed using randomly sampled images from type Ib boutons with a diameter >2 μm (to ensure the exclusion of type Is boutons). The diameter of synaptic vesicles and cisternae were measured from the outside of the vesicle membrane along the long axis. A vesicle was measured only if its borders were well defined and it had a clear center (i.e., it was not a dense-core vesicle). Structures larger than 60 nm in diameter were excluded from calculations of mean synaptic vesicle diameter. High K^+ stimulation was performed using a modified Jan and Jan solution (Jan and Jan, 1976; 45 mM NaCl, 90 mM KCl, 36 mM sucrose, 2 mM $CaCl_2$, 2 mM $MgCl_2$, and 5 mM HEPES, pH 7.3). Cisternae were defined as intracellular single-membrane structures with a diameter greater than or equal to 80 nm. In certain cases, the exact size of a cisterna could not be measured; however, if a cisterna clearly was >80 nm in diameter, it was included in the analysis of the number of cisternae per unit area (see Figs. 6, 8). The analysis was done blind to genotype whenever possible. Measurements were performed using ImageJ (NIH) and Adobe Photoshop (Adobe Systems) software.

FM1–43 staining. Wandering third instar larvae were dissected in HL3.1 solution with 1 mM $CaCl_2$ and the motor nerves were severed to

prevent spontaneous muscle contractions. Larvae were stimulated for 5 min with high K^+ (90 mM) Jan and Jan solution containing 4 μM FM1–43 (Invitrogen). Preparations were washed in standard HL3.1 and briefly incubated in HL3.1 saline containing 100 μM Advasep-7 (Biotium), which has been shown to reduce background fluorescence (Kay et al., 1999). Larvae were washed again in HL3.1 and then imaged to quantify the level of FM1–43 uptake. After 10 min, the neuromuscular junction (NMJ) was imaged a second time, then immediately incubated for 1 min with high K^+ (90 mM) Jan and Jan solution, washed, and imaged a final time to determine the extent of unloading. For frequency-induced FM1–43 unloading, preparations were stained with 4 μM FM1–43 as described above and stimulated for 10 min at 1 Hz. Image acquisition was performed using an UltraVIEW VoX confocal imaging system (PerkinElmer) equipped with an ImagEM camera (C9100–13; Hamamatsu) and a Yokogawa CSU-X1 spinning disk head. Images were acquired as a *Z* series taken at 0.3 μm steps using a 40× water-immersion objective. Mean bouton intensity was determined using Volocity 3D Image Analysis Software (PerkinElmer). Background intensity of the surrounding region was subtracted from bouton labeling.

Electrophysiology. Postsynaptic currents were recorded at segment A3 of ventral longitudinal muscle 6 in third instar larvae using two-electrode voltage-clamp with a −80 mV holding potential in HL3.1 solution. The final Ca^{2+} concentration was adjusted to the desired level indicated in the text. Data acquisition and analysis were performed using Axoscope 9.0 and Clampfit 9.0 software (Molecular Devices). Quantal content was estimated by dividing the current integral of nerve-evoked currents by the current integral from individual quanta as previously described (Barber et al., 2009). Motor nerves innervating the musculature were severed and placed into a suction electrode so action potential stimulation could be applied at the indicated frequencies using a programmable stimulator. Statistical analysis was performed using GraphPad Prism for Mac OS X version 5.0a and Origin Software (OriginLab). Statistical significance was determined using two-tailed Student's *t* tests or one-way ANOVA and noted as follows: $*p < 0.05$; $**p < 0.01$; $***p < 0.001$. For all data, error bars indicate SEM.

Results

Evolutionary analysis of synaptogyrin and synaptophysin

Synaptogyrin and synaptophysin have previously been established as evolutionarily conserved proteins (Hübner et al., 2002; Sánchez-Pulido et al., 2002; Abraham et al., 2006). We were interested in examining the emergence of these and several additional MARVEL domain-containing proteins in relation to other synaptic vesicle components. While many synaptic vesicle proteins such as v- and t-SNAREs, the vacuolar ATPase, and Rab 3 are ancient eukaryotic proteins, several key proteins involved in neurotransmitter exocytosis emerged more recently in evolution (Srivastava et al., 2010). For example, synaptotagmin 1 and complexin homologs are absent in the yeast *Saccharomyces cerevisiae* and the amoeba *Dictyostelium discoideum*, but are present in the placozoan *Trichoplax adhaerens*, a simple multicellular organism that lacks a nervous system, but has several organized cell layers (Srivastava et al., 2008; Barber et al., 2009). A reciprocal protein-protein BLAST search revealed synaptogyrin and synaptophysin orthologs in the *T. adhaerens* genome, indicating that they too evolved before the emergence of defined synapses (Table 1). Interestingly, while the *S. cerevisiae* genome lacks synaptogyrin or synaptophysin orthologs, we were able to identify a putative synaptogyrin family member in the unicellular choanoflagellate *M. brevicollis* with 33% identity to human synaptogyrin 1 and four predicted transmembrane domains (King et al., 2008). Our BLAST search did not reveal a *M. brevicollis* synaptophysin homolog, raising the possibility that the synaptogyrin and synaptophysin families (gyrins and physins, respectively) are descended from an ancestral synaptogyrin-like protein. Since choanoflagellates are thought to be the closest extant unicellular relative of metazoans (King et al., 2008), the presence of a synaptogyrin-like ortholog in *M. brevicollis* but not in yeast suggests a unique role for synaptogyrin in early metazoan evolution. This putative *M. brevicollis* synaptogyrin ortholog is almost entirely comprised of the MARVEL domain, with its short N and C termini each predicted to be <15 aa in length. Therefore, it is likely that the MARVEL domain itself has an important cellular function and that the N and C termini of gyrins and physins may have elaborated and adapted over the course of evolution to perform a variety of specialized tasks in other organisms. Interestingly, we were unable to identify a gyrin ortholog in the sea anemone *Nematostella vectensis*, but did uncover at least one physin ortholog, suggesting that some metazoans do not require both proteins or that the functions of physins and gyrins are interchangeable (Putnam et al., 2007).

Table 1. Evolutionary conservation of selected MARVEL domain and SCAMP proteins

	Vertebrates		Arthropod		Nematodes	Cnidarians	Placozoan	Choanoflagellates	Fungi
	M.m.	D.r.	D.m.	T.c.	(C.e.)	(N.v.)	(T.a.)	(M.b.)	(S.c.)
Gyrin	+	+	+	+	+	−[a]	+	+	−
Physin	+	+	−[b]	+	+	+	+	−	−
CMTM	+	+	+	+	+	+	?[c]	−	−
Occludin	+	+	−	−	−	−	−	−	−
MAL	+	+	−	−	−	−	−	−	−
MYADM	+	+	−	−	−	−	−	−	−
SCAMP	+	+	+	+	+	+	+	+	−

+, Homolog; −, no homolog; M.m., *Mus musculus*; D.r., *Danio rerio*; D.m., *Drosophila melanogaster*; T.c., *Tribolium* castaneum; C.e., *Caenorhabditis elegans*; N.v., *Nematostella vectensis*; T.a., *Trichoplax adhaerens*; M.b., *Monosiga brevicollis*; S.c., *Saccharomyces cerevisiae*.

[a]N.v. has no gyrin homolog, but it does have two physin-like homologs.

[b]No sequenced *Drosophila* species has a physin homolog.

[c]BLAST using mouse CMTM 4 identified a potential T.a. homolog with a partial MARVEL domain, but this protein has only three predicted transmembrane domains.

We also searched for homologs of several other MARVEL domain-containing proteins and found that some, including MAL (myelin and lymphocyte protein), MYADM (myeloid-associated differentiation marker gene), and occludin (a component of tight junctions), are absent from invertebrate genomes. This lack of conservation is unsurprising given that vertebrate myelin and the myelin-like sheaths found in some invertebrates are hypothesized to have arisen through convergent evolution (Hartline and Colman, 2007). Similarly, invertebrates do not have tight junctions, but rather have analogous structures known as septate junctions (Furuse and Tsukita, 2006). We also examined the CMTM family (CKLF-like MARVEL transmembrane domain-containing family, where CKLF stands for chemokine-like factor), a novel group of proteins with a highly conserved member named CMTM4 that has been implicated in regulating the cell cycle and cellular growth (Plate et al., 2010). CMTM4 homologs are found in *Drosophila*, *C. elegans*, *N. vectensis*, and potentially in *T. adhaerens*, although this putative homolog has only three predicted transmembrane domains. Finally, we investigated the evolutionary conservation of the secretory carrier-associated membrane proteins (SCAMPs), which lack the MARVEL domain, but have the same tetraspanning membrane topology (Hubbard et al., 2000). Interestingly, SCAMP homologs are also found in the plant kingdom, suggesting they perform a more ubiquitous role in multicellular organisms (Fernández-Chacón and Südhof, 2000).

The *D. melanogaster* genome encodes a single synaptogyrin homolog (CG10808) that is 42% identical to human synaptogyrin 1 (Fig. 1). Unlike many other invertebrates, including *C.*

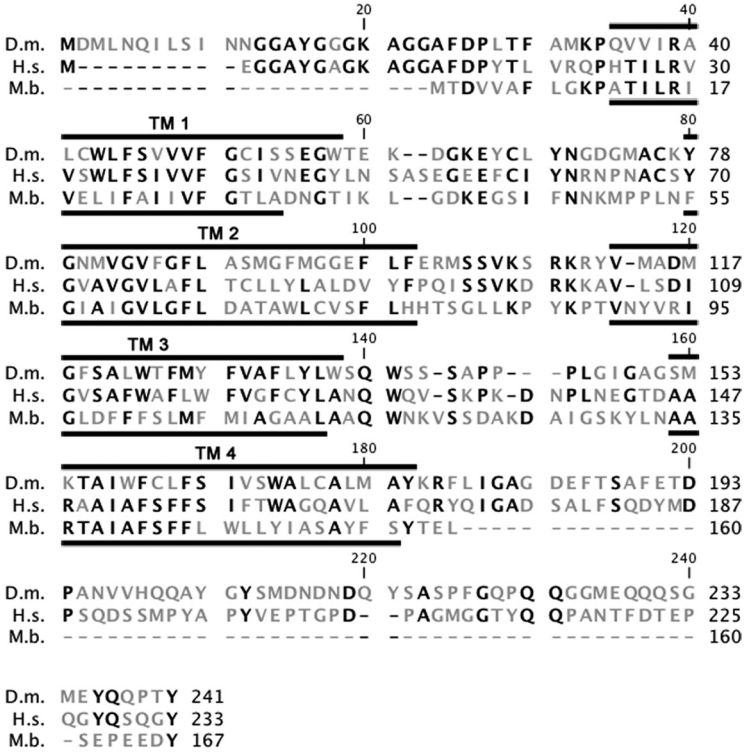

Figure 1. Protein sequence alignment of synaptogyrin homologs. Transmembrane (TM) domains are indicated for *Drosophila* synaptogyrin (bars above the alignment) and *M. brevicollis* synaptogyrin (bars below the alignment). Conserved residues are indicated in black. Sequence abbreviations: D.m., *Drosophila melanogaster*; H.s., *Homo sapiens*; M.b., *Monosiga brevicollis*.

elegans and the red flour beetle *Tribolium castaneum*, all of the sequenced *Drosophila* species lack a synaptophysin ortholog. However, the *D. melanogaster* genome does encode other MARVEL domain-containing proteins, including a CMTM4 ortholog (CG15211) and Singles Bar (CG13011), a protein involved in myoblast fusion (Estrada et al., 2007). In *C. elegans*, synaptophysin expression is largely restricted to muscle cells in the pharynx and anal sphincter (Abraham et al., 2006), while synaptogyrin is expressed in most neurons (Nonet, 1999; Abraham et al., 2011), indicating that synaptogyrin is likely to be the predominant synaptic vesicle MARVEL protein in nematodes.

Synaptogyrin is not an essential protein in *Drosophila*

Synaptogyrin has not previously been characterized in *Drosophila*. Therefore, we examined the localization of endogenous synaptogyrin by generating antisera against a recombinant C-terminal fusion protein of *Drosophila* synaptogyrin. As expected for a presumptive synaptic vesicle protein, immunohistochemistry of third instar *Drosophila* larvae reveals abundant synaptogyrin expression throughout the brain and ventral nerve cord (Fig. 2*A*). Synaptogyrin is also found at the larval NMJ, where it strongly colocalizes with the synaptic vesicle protein synaptotagmin 1 (Syt1) and partially overlaps with the active zone protein bruchpilot (Fig. 2*B*,*C*). Similarly, expression of a GFP-tagged synaptogyrin transgene in neurons using the *elav^{c155}-GAL4* driver resulted in presynaptic targeting at the NMJ that overlapped with Syt1 labeling (Fig. 2*D*). We conclude that, like the murine and worm synaptogyrin homologs, *Drosophila* synaptogyrin is a presynaptic neuronal protein.

We next sought to investigate the function of *Drosophila* synaptogyrin by generating a *synaptogyrin (gyr)*-null mutant. We isolated two independent partial deletions of the *synaptogyrin* genomic locus via imprecise excision of a P-element (P{lacW}l(2)SH0644^{SH0644}) located just upstream of the *synaptogyrin* translation start site. The first deletion, *gyr^1*, extends 2.5 kb into the *synaptogyrin* locus and removes the first two exons and a portion of the third exon, while the second deletion, *gyr^2*, is a smaller 1.7 kb deletion that removes the first exon (Fig. 3*A*). A precise excision line, *gyr^{PE}*, was chosen to serve as a control for genetic background in all experiments. The extent of the deletions and the precise excision event were confirmed by PCR and sequencing. Western analysis revealed the complete absence of synaptogyrin immunoreactivity in both *gyr^1* and *gyr^2* animals (Fig. 3*B*). Similarly, synaptogyrin staining is absent at the larval NMJ in mutant animals (Fig. 3*C*). The antibody raised against synaptogyrin targets the C terminus of the protein that is left intact in both deletions, indicating that a truncated version of the protein is not produced. We conclude that *gyr^1* and *gyr^2* represent null mutations in the *synaptogyrin* locus. Unless otherwise noted, *gyr^1* animals were used in all experiments. In agreement with mouse and *C. elegans* knock-outs, *Drosophila gyr* mutant animals are viable, fertile, and appear behaviorally normal. They develop at a similar rate and have a normal life span compared with control animals (data not shown). Motor function and coordination appear to be unaffected at both the larval and adult stages. Additionally, *gyr* males are capable of performing all aspects of the *Drosophila* courtship ritual and display a normal courtship index (data not shown). Therefore, we conclude that synaptogyrin is not essential for viability, fertility, or basic motor functions in *Drosophila*.

gyr mutants have normal synaptic growth and synaptic architecture

As *Drosophila* proceed through the larval stages, the surface area of the body wall muscles increases ~100-fold, and synaptic innervation at the NMJ increases in parallel through the addition of new boutons to maintain proper muscle depolarization. Disruptions in *trans*-synaptic growth signaling pathways (e.g., Wnt or TGFβ) or alterations in synaptic activity levels can lead to synaptic undergrowth or overgrowth (Budnik et al., 1990; Guan et al., 2005; Collins and DiAntonio, 2007). Furthermore, many *Drosophila* endocytic and membrane recycling mutants, including *rab11*, *endophilin*, *synaptojanin*, and *dap160*, display an increase in supernumerary or "satellite" boutons (Koh et al., 2004; Dickman et al., 2006; Khodosh et al., 2006). At *gyr* NMJs, overall synaptic morphology is normal with no obvious overgrowth, undergrowth, or satellite bouton phenotypes. The total number of synaptic boutons at muscle 6/7 of segment A3 is unchanged in both *gyr^1* and *gyr^2* mutants compared with controls (Fig. 4*A*,*B*; $p = 0.48$, one-way ANOVA). There also is no significant difference in muscle size, consistent with our previous observation that *gyr* mutants do not have developmental delays (control = 56,000 $\pm$ 1800 μm^2, $n = 22$; *gyr^1* = 61,000 $\pm$ 2200 μm^2, $n = 23$; *gyr^2* = 59,000 $\pm$ 2000 μm^2, $n = 20$; $p = 0.20$, one-way ANOVA). Similarly, the number of active zones as defined by nc82 staining

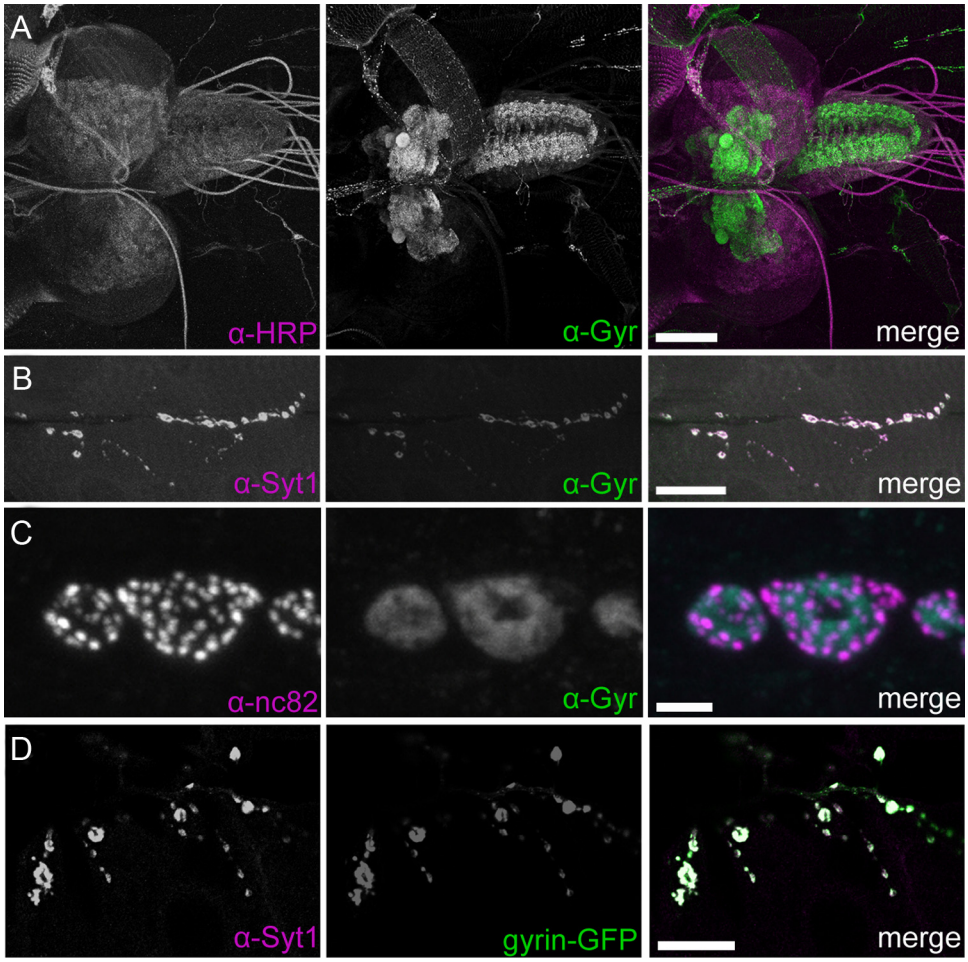

Figure 2. Synaptogyrin localization at synapses. ***A***, Immunohistochemistry with antisera against the neuronal membrane marker HRP (magenta) and synaptogyrin (Gyr, green) indicates that synaptogyrin is broadly expressed in the synaptic neuropil of the larval CNS. ***B***, Synaptogyrin (green) is expressed presynaptically at the larval NMJ where it colocalizes with synaptotagmin 1 (Syt1, magenta). ***C***, Synaptogyrin is not confined to active zones, which are indicated by nc82 staining (magenta). ***D***, Synaptogyrin-GFP (gyrin-GFP, green) driven by the pan-neuronal driver *elav*^{c155}*-GAL4* localizes to synapses. Scale bars: ***A***, 100 μm; ***B***, 25 μm; ***C***, 2 μm; ***D***, 20 μm.

is unchanged in *gyr*^{1}, with no noticeable alterations in active zone size or spacing (Fig. 4*C*,*D*; control = 529 ± 24.4, $n = 14$; *gyr* = 510 ± 28.7, $n = 14$, $p = 0.61$). We conclude that the loss of synaptogyrin in *Drosophila* does not significantly alter synaptic growth or influence the number of synaptic vesicle release sites.

Ultrastructural analysis reveals alterations in synaptic vesicle diameter and density

Although bouton morphology appears normal at the light microscopy level in *gyr* mutants, ultrastructural analysis by TEM of type Ib boutons reveals several abnormalities in *gyr* animals. In particular, boutons at the larval NMJ in *gyr* animals display variable changes in synaptic vesicle diameter and density. In control boutons, synaptic vesicles are uniform in size and cluster around the periphery of the bouton (Fig. 5*A*,*B*). Synaptic vesicle diameter and density in some *gyr* boutons appear similar to controls (Fig. 5*E*). However, other *gyr* boutons (~30–40%) have an increase in the number of large synaptic vesicles, the largest of which may represent endosomes or endocytic cisternae (Fig. 5*C*,*D*). This dramatic increase in the variability of synaptic vesicle diameter in certain *gyr* boutons is illustrated in Figure 5*D* (compare Fig. 5*B*). A few (~10%) *gyr* boutons have a marked decrease in synaptic vesicle density (Fig. 5*F*), and while many *gyr* boutons appear normal, overall there is a slight but statistically significant decrease in the density of synaptic vesicles (Fig. 5*G*; control = 131.7 ± 9.4 vesicles/μm^2, $n = 21$; *gyr* = 101.5 ± 9.5 vesicles/μm^2, $n = 21$; $p = 0.03$). In contrast, there is a statistically significant increase in mean synaptic vesicle diameter in *gyr* boutons compared with controls (Fig. 5*H*; control = 42.7 ± 0.50 nm, *gyr* = 45.2 ± 0.93 nm; $p = 0.02$). There is also an overall shift in the distribution of synaptic vesicle diameter toward larger values, with an increased variability in diameter, suggesting synaptogyrin directly or indirectly regulates synaptic vesicle size (Fig. 5*I*).

gyr mutants retain endocytic cisternae following intense stimulation

Synaptic vesicles are known to form through several pathways, including traditional clathrin-mediated endocytosis from the plasma membrane (De Camilli and Takei, 1996) and via endosomal intermediates (Heuser and Reese, 1973; Takei et al., 1996; de Lange et al., 2003). During periods of relatively low activity, clathrin-mediated endocytosis appears to be the predominant form of synaptic vesicle retrieval at central synapses (Granseth et al., 2006). However, tetanic stimulation or intense nonphysiological stimuli can induce bulk endocytosis, a process whereby large plasma membrane invaginations are internalized to form endocytic cisternae from which synaptic vesicles then bud (Miller and Heuser, 1984; Richards et al., 2000; Richards et al., 2003;

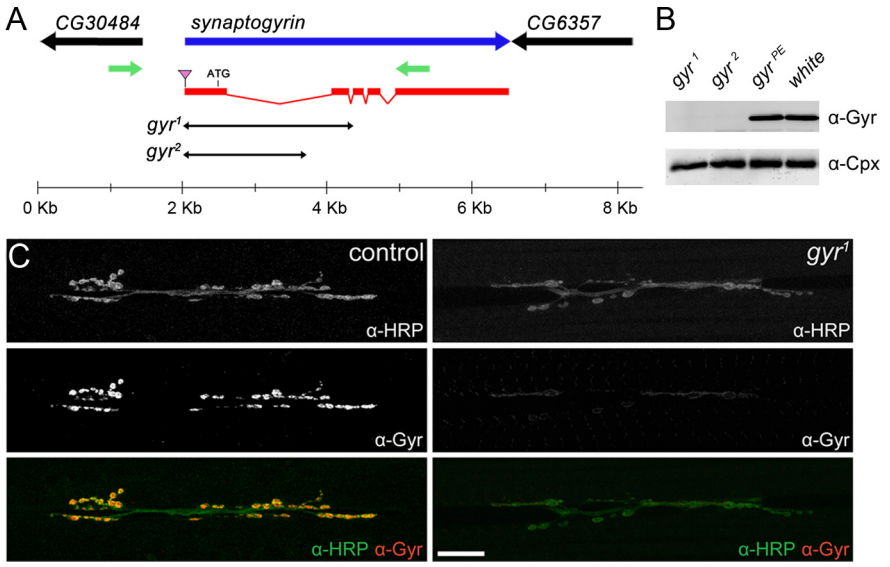

Figure 3. Generation of a *Drosophila synaptogyrin* (*gyr*) mutant. ***A***, The *synaptogyrin* locus is diagrammed with the two neighboring genes (CG30484 and CG6357). The location of the P-element used for the excision screen is indicated by the pink triangle. Two separate deletions were isolated and are indicated by black lines. The green arrows mark the locations for the PCR primers used to determine the extent of each deletion. ***B***, Western blot analysis of synaptogyrin protein expression levels from homogenates made from *white*, gyr^{PE}, gyr^{1}, and gyr^{2} adult heads. Complexin (Cpx) immunoreactivity was used as a loading control. Synaptogyrin immunoreactivity is completely absent in gyr^{1} and gyr^{2}. ***C***, Immunohistochemistry at third instar larval NMJs confirms that synaptogyrin (red) is absent in the gyr^{1} mutant but not in the control (gyr^{PE}). Synaptic varicosities were identified using α-HRP antibodies (green).

Evans and Cousin, 2007). The presence of many large, endosomal-like structures in a subset of *gyr* mutant boutons prompted us to test if synaptic vesicle recycling via endosomal intermediates was disrupted in these boutons, resulting in a buildup of endocytic cisternae.

To test this hypothesis, we incubated larvae with a high K^+ solution known to induce the formation of endocytic cisternae in response to strong synaptic vesicle exocytosis caused by continuous membrane depolarization (Marxen et al., 1999; de Lange et al., 2003; Akbergenova and Bykhovskaia, 2009). We then investigated whether *gyr* mutants were impaired in recovering vesicle membrane via bulk endocytosis or in resolving endocytic cisternae into synaptic vesicles. Under normal resting conditions, *gyr* mutants have a statistically significant increase in the number of cisternae per μm^2 (cisternae are defined as structures with a diameter >80 nm; Fig. 6 [left]; control = 0.53 ± 0.10 cisternae/μm^2, $n = 21$; *gyr* = 1.57 ± 0.33 cisternae/μm^2, $n = 23$; $p < 0.01$). Immediately after a 5 min incubation in high K^+ (90 mM) Jan and Jan solution (Jan and Jan, 1976; Akbergenova and Bykhovskaia, 2009), both control and *gyr* animals show a similar increase in the number of cisternae, suggesting that *gyr* mutants are not impaired in this step of bulk endocytosis (Fig. 6 [center]; control = 15.0 ± 0.62 cisternae/μm^2, $n = 8$; *gyr* = 12.7 ± 2.0 cisternae/μm^2, $n = 5$; $p = 0.21$). However, when larvae are subsequently allowed to recover for 10 min in normal (low K^+) HL3.1 saline before fixation, *gyr* animals have a significantly higher amount (~50% by area) of endocytic cisternae remaining compared with controls (Fig. 6 [right]; control = 5.35 ± 0.81 cisternae/μm^2, $n = 21$; *gyr* = 8.26 ± 0.77 cisternae/μm^2, $n = 22$; $p = 0.01$). We confirmed by serial EM reconstruction of several cisternae that these membrane compartments are not connected to the plasma membrane, and thus do not represent membrane infoldings (data not shown). These observations suggest that the process of resolving synaptic vesicles from endocytic cisternae is delayed in *gyr* mutants. To examine cisternae following intense nerve stimulation, we treated larvae with a protocol that included 10 trains at 100 Hz (each lasting 1 s with a 1 s gap between each pulse for a total of 1000 stimuli) and fixed the preparations immediately afterward for EM analysis. *gyr* boutons showed a significantly higher number of cisternae compared with control boutons following stimulation (control = 0.29 ± 0.17 cisternae/μm^2, $n = 9$; *gyr* = 1.24 ± 0.29 cisternae/μm^2, $n = 15$; $p = 0.03$).

To further examine synaptic vesicle recycling, we turned to the styryl dye FM1–43, which reversibly binds membranes and increases in fluorescence intensity upon membrane integration, allowing one to track compartments as they move through the exo-endocytic cycle (Cochilla et al., 1999). Mutations in a variety of endocytic proteins, such as endophilin, eps15, synaptojanin, and dap160, result in decreased loading of FM1–43 dye (Verstreken et al., 2002, 2003; Koh et al., 2004, 2007). When we incubated *gyr* and control larvae for 5 min with 90 mM K^+ Jan and Jan solution containing 4 μM FM1–43, we found no significant difference in the amount of dye uptake (Fig. 7*A–C*; control = 13,600 ± 400 A.U.; *gyr* = 13,700 ± 600 A.U.; $p = 0.83$). This result is consistent with our EM results that demonstrate *gyr* boutons are capable of taking up large quantities of membrane in the form of endocytic cisternae immediately following a K^+ shock (Fig. 6). We also examined the capacity of *gyr* and control boutons to unload dye after 10 min of rest in normal saline to determine whether exocytosis is significantly impaired. A 1 min incubation with high K^+ saline resulted in a similar level of destaining relative to loading fluorescence levels (control = 31.1 ± 2.40% of loading fluorescence, $n = 13$ NMJs; *gyr* = 37.9 ± 2.50%, $n = 11$ NMJs, $p = 0.06$), indicating that *gyr* boutons are not defective in releasing FM1–43. Since unloading was performed with an intense, nonphysiological stimulus, this assay is poorly suited to determine whether *gyr* mutants sequester FM1–43 in endocytic cisternae to a greater extent than controls. The second high K^+ stimulus used to unload the dye may have caused cisternae to fuse in addition to synaptic vesicles, which would mask any defect in synaptic vesicle budding from cisternae. To bypass this problem, we quantified bouton fluorescence intensity 10 min after loading during a rest period where only spontaneous vesicle release occurs, allowing a more sensitive measure for vesicle availability following intense stimulation. Under these conditions, we found that *gyr* boutons retain a higher percentage of dye relative to controls (Fig. 7*C*; control = 90.8 ± 1.83% of loading fluorescence, $n = 13$ NMJs; *gyr* = 98.9 ± 1.48%, $n = 11$ NMJs; $p < 0.01$), consistent with the observation that *gyr* mutants are delayed in resolving synaptic vesicles from cisternae. To directly assay whether *gyr* boutons are defective in vesicle availability following a milder stimulation protocol, we examined FM1–43 unloading after 10 min of stimulation at 1 Hz (Fig. 7*D–F*). Using this stimulation protocol for unloading, we observed a significantly higher level of fluorescence intensity re-

tained in *gyr* boutons compared with control preparations (control = 34.4 ± 3.28%, $n = 19$ NMJs; *gyr* = 45.6 ± 4.47%, $n = 18$ NMJs; $p < 0.05$).

If synaptogyrin regulates synaptic vesicle budding from endocytic cisternae, synaptic vesicle recycling induced by high K^+ stimulation might exacerbate the misregulation of synaptic vesicle size seen in *gyr* mutants under nonstimulated conditions. However, when we measured the diameter of synaptic vesicles 10 min after high K^+ stimulation, we found that the distribution of synaptic vesicle diameter was more similar to controls compared with pre-K^+ stimulation (Fig. 8*A*,*B*). The average synaptic vesicle diameter following the K^+ shock was not significantly different between *gyr* and controls (Fig. 8*C*,*D*; control = 43.33 ± 0.58 nm, $n = 18$ boutons; *gyr* = 43.28 ± 0.49 nm, $n = 20$ boutons; $p = 0.95$), and individual *gyr* boutons had much less variation in their mean synaptic vesicle diameter (Fig. 8*D*). So while the number of large cisternae is increased in *gyr* mutants after intense stimulation, synaptic vesicles (<60 nm in diameter) that form soon after stimulation are more similar in size to controls (Fig. 8*D*). These findings suggest that intense stimulation results in the restoration of normal synaptic vesicle diameter immediately after the stimulus, likely by forcing abnormally large synaptic vesicles to fuse.

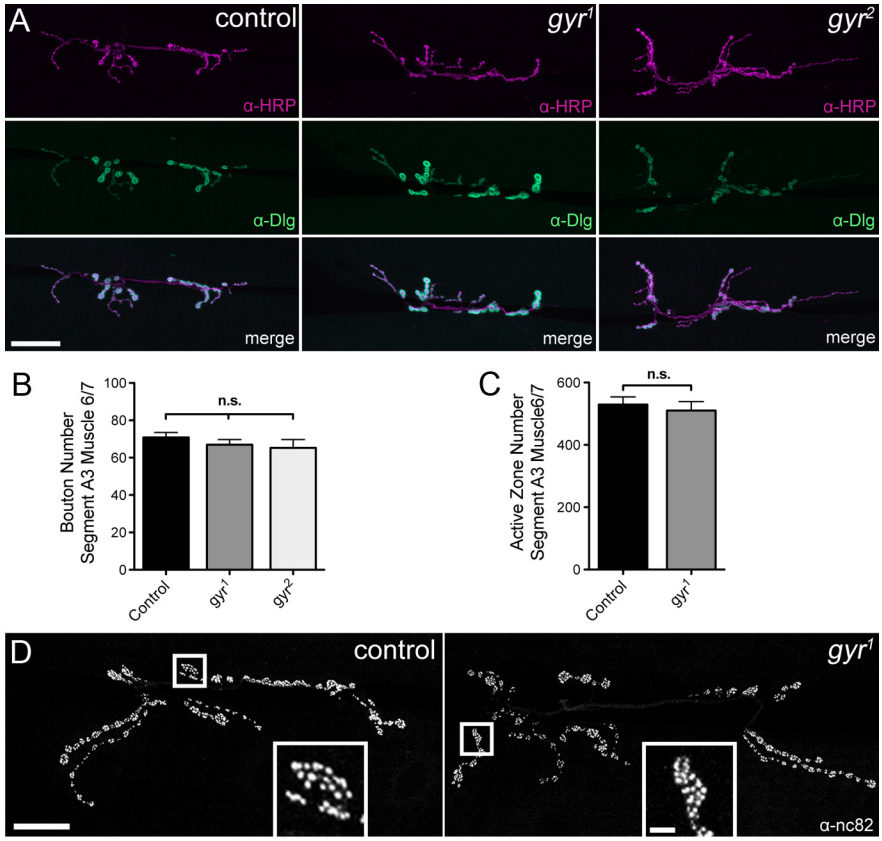

Figure 4. The number of synaptic varicosities and active zones is unchanged in *gyr* mutants. ***A***, Synaptic bouton number and morphology at muscle 6/7 in body segment A3 are normal in gyr^1 and gyr^2 third instar larvae relative to controls (gyr^{PE}), as determined by immunostaining against HRP (magenta) and Discs large (Dlg), a postsynaptic scaffolding protein (green). ***B***, Quantification of total bouton number at muscle 6/7 revealed no significant difference between control, gyr^1, and gyr^2 ($p = 0.48$, one-way ANOVA). Average total bouton number ± SEM: control = 70.8 ± 2.6, $n = 23$; gyr^1 = 66.9 ± 2.8, $n = 22$; gyr^2 = 65.2 ± 4.5, $n = 21$. ***C***, Active zone number is not significantly different in *gyr* compared with controls ($p = 0.61$). Average active zone number ± SEM: control = 529 ± 24.4, $n = 14$; *gyr* = 510 ± 28.7, $n = 14$. ***D***, Representative images of control and *gyr* NMJs stained with the active zone marker nc82. Boxed areas are shown at higher magnification. Scale bars: ***A***, 40 μm; ***D***, 20 μm; ***D*** (inset), 2.5 μm.

To further investigate recycling through endosomal intermediates, we used the temperature-sensitive dynamin mutant *shibire* (shi^{ts1}) in combination with *gyr* to examine the recovery of synaptic vesicles following a complete endocytic block. In shi^{ts1} larvae, synaptic vesicles are depleted and synapses accumulate numerous collared pits and membrane invaginations at restrictive temperatures. Upon subsequent recovery at the permissive temperature, cisternae are generated from which synaptic vesicles then bud (Koenig and Ikeda, 1996). We repeated the previously described high K^+ incubation with shi^{ts1}; gyr^1 and shi^{ts1}; gyr^{PE} larvae at 32°C and allowed larvae to recover at room temperature (~22°C) in low K^+ saline before fixation for EM. Ten minutes after a 5 min simultaneous heat shock and K^+ stimulation, both shi^{ts1}; gyr^1 and shi^{ts1}; gyr^{PE} boutons contained numerous overlapping and misshapen cisternal-like structures that were difficult to measure, therefore we extended the recovery period to 20 min. We found that shi^{ts1}; gyr^{PE} and shi^{ts1}; gyr^1 boutons contained a significantly greater number of cisternae compared with poststimulation non-*shibire* larvae ($p < 0.05$), suggesting that the inhibition of dynamin activity significantly impacts endocytic recovery through bulk endocytosis following K^+ stimulation. Furthermore, as was the case in the absence of dynamin inhibition, shi^{ts1} larvae carrying the *gyr* mutation tended to have more cisternae than shi^{ts1} controls, although this difference was not statistically significant (Fig. 8*E*,*F*; shi^{ts1}; gyr^{PE} = 8.63 ± 1.2 cisternae/μm^2, $n = 14$; shi^{ts1}; gyr^1 = 10.92 ± 0.87 cisternae/μm^2, $n = 17$; $p = 0.13$). Interestingly, shi^{ts1}; gyr^1 boutons had a dramatic increase (>2-fold) in very large (>200 nm) endocytic structures, while shi^{ts1}; gyr^{PE} boutons at 20 min poststimulation had values more similar to those seen in gyr^{PE} and gyr^1 larvae 10 min after stimulation (Fig. 8*G*; shi^{ts1}; gyr^{PE} = 0.66 ± 0.22 cisternae/μm^2, $n = 14$; shi^{ts1}; gyr^1 = 1.58 ± 0.31 cisternae/μm^2, $n = 17$; $p = 0.03$). This is likely a consequence of dynamin inhibition forcing a greater fraction of synaptic vesicle membrane to recycle through cisternae via the bulk endocytosis pathway, thereby exacerbating the *gyr* phenotypes. Indeed, we observed that synaptic vesicle diameter in shi^{ts1}; gyr^1 larvae poststimulation reverted to values similar to those observed in *gyr* larvae prestimulation, suggesting that these boutons again become defective in regulating synaptic vesicle size when bulk endocytosis contributes prominently to the recovery of synaptic vesicles (Fig. 8*D*). Intriguingly, when we quantified synaptic vesicle density poststimulation, we discovered that both *gyr* and control non-*shibire* larvae recovered to levels similar to those seen before stimulation within 10 min (Fig. 8*H*; control = 125.8 ± 10.6 vesicles/μm^2, $n = 18$; *gyr* = 131.1 ± 8.1 vesicles/μm^2, $n = 21$; $p = 0.69$). However, at 20 min poststimulation, shi^{ts1}; gyr^{PE} and shi^{ts1}; gyr^1 boutons still had a large decrease in synaptic vesicle density compared with control and *gyr*, and shi^{ts1}; gyr^1 larvae had significantly lower density than shi^{ts1}; gyr^{PE} (Fig. 8*H*; shi^{ts1}; gyr^{PE} = 80.6 ± 7.7 vesicles/μm^2, $n = 14$; shi^{ts1}; gyr^1 = 51.8 ± 4.0 vesicles/μm^2, $n = 17$; $p < 0.01$). While the *shibire* muta-

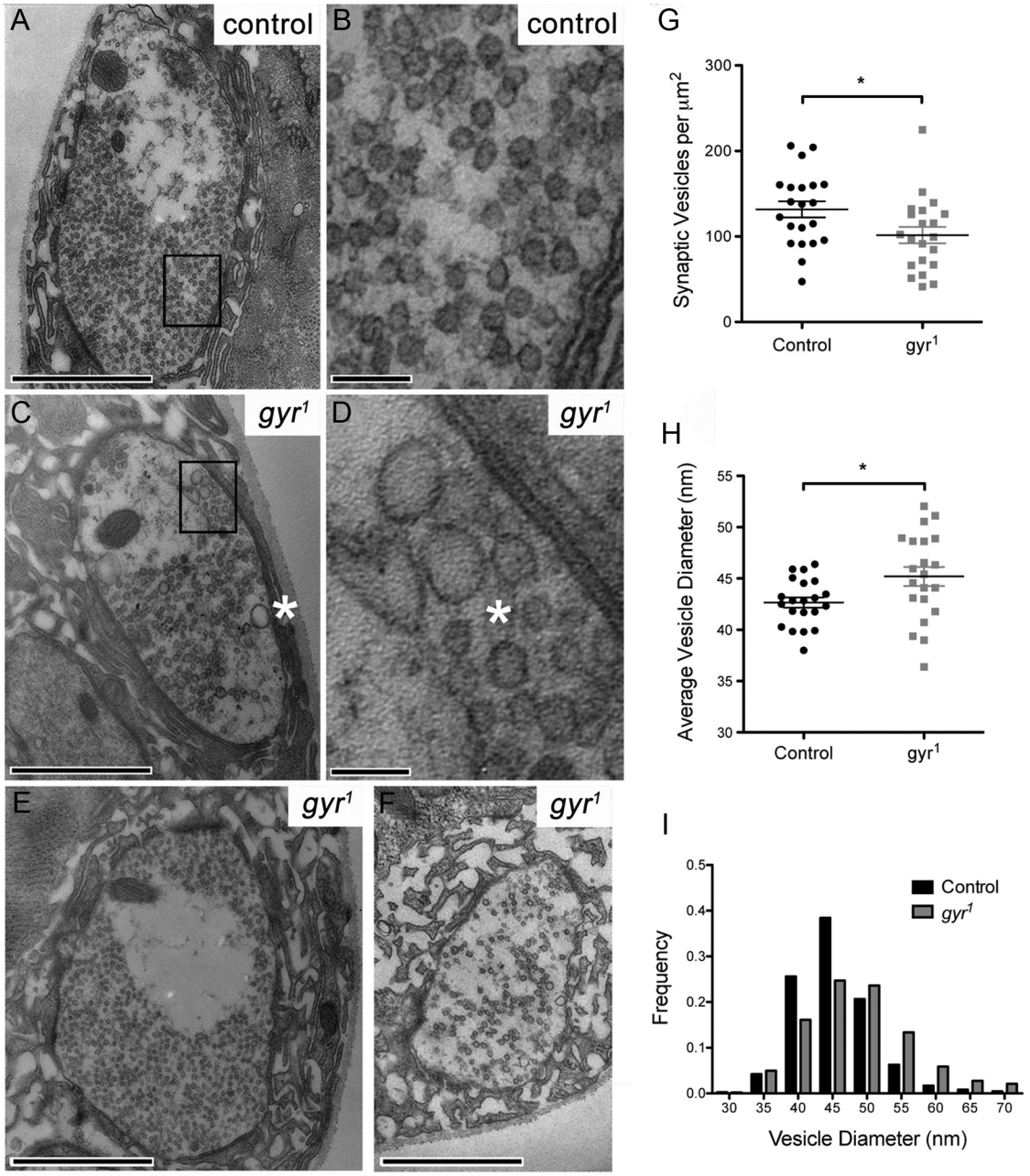

Figure 5. Ultrastructural analysis reveals alterations in synaptic vesicle diameter in *gyr* mutants. ***A***, Representative image of a type Ib synaptic bouton from a control larva. ***B***, The boxed region in ***A*** is shown at higher magnification to illustrate homogeneity of synaptic vesicle diameter in control animals. ***C***, Example of a *gyr* bouton with abnormal synaptic vesicle diameter and large cisternal-like structures (indicated by asterisk). ***D***, The boxed region in ***C*** is shown at higher magnification to illustrate the variability in synaptic vesicle diameter (see asterisk). ***E***, Representative *gyr* bouton with similar synaptic vesicle diameter and density relative to controls. ***F***, Example of a *gyr* bouton with decreased synaptic vesicle density. ***G***, Synaptic vesicle density is significantly decreased in *gyr* mutants compared with controls ($p = 0.03$). Each point on the graph represents the synaptic vesicle density of a single bouton. Average synaptic vesicle density per bouton area (μm^2) ± SEM: control = 131.7 ± 9.4, $n = 21$; *gyr* = 101.5 ± 9.5, $n = 21$; $p = 0.03$. ***H***, The average synaptic vesicle diameter (vesicles < 60 nm in diameter) is increased in *gyr* mutants relative to controls ($p = 0.02$). Each data point represents the average synaptic vesicle diameter for a single bouton. At least 20 synaptic vesicles were measured in each bouton to obtain the mean synaptic vesicle diameter. Average synaptic vesicle diameter (in nanometers) ± SEM: control = 42.7 ± 0.50, $n = 21$ boutons; *gyr* = 45.2 ± 0.93, $n = 21$ boutons. ***I***, Synaptic vesicle diameter is shifted to higher values relative to the control in *gyr* mutant larvae. Since varying numbers of synaptic vesicles were measured in each bouton, the frequency distribution of each bouton was calculated and normalized to obtain the overall frequency distribution. Scale bars: ***A***, ***C***, ***E***, ***F***, 1 μm; ***B***, ***D***, 100 nm.

tion alone inhibits endocytic recovery following synaptic vesicle depletion, the combination of *shibire* and *gyr* dramatically enhances this phenotype, indicating synaptogyrin plays an important role in modulating synaptic vesicle regeneration via endocytic cisternae following intense stimulation.

gyr mutants exhibit alterations in presynaptic function

The increase in synaptic vesicle diameter seen in *gyr* mutants under resting conditions raises the possibility that there may be a concomitant change in quantal size. Indeed, postsynaptic recordings of spontaneous miniature excitatory junctional currents (mEJCs or minis) in third instar larvae using two-electrode voltage-clamp revealed a significant increase in quantal size in the *gyr* mutant (Fig. 9*A*; control = 0.83 ± 0.09 nA, $n = 5$; *gyr* = 1.35 ± 0.11 nA, $n = 6$; $p < 0.01$). *gyr* larvae also display a slight but significant decrease in spontaneous mEJC frequency (Fig. 9*B*; control = 2.4 ± 0.2 Hz, $n = 5$; *gyr* = 1.8 ± 0.1 Hz, $n = 6$; $p < 0.05$). Presynaptic expression of synaptogyrin using the *elav*^{c155}-

GAL4 driver restored both mEJC amplitude and frequency to wild-type values (Fig. 9*A*,*B*; mini amplitude = 0.75 ± 0.18 nA, $n = 4$; mini frequency = 2.6 ± 0.3 Hz, $n = 4$). While mEJC amplitude is increased in *gyr*, there is no significant change in evoked EJC amplitude at 0.2 mM Ca^{2+} (control = 4.1 ± 0.1 nA, $n = 5$; *gyr* = 3.8 ± 0.1 nA, $n = 6$; $p > 0.05$), indicating that quantal content is reduced in *gyr* mutants (Fig. 9*C*; control = 5.1 ± 0.4 quanta, $n = 5$; *gyr* = 3.2 ± 0.3 quanta, $n = 6$; $p < 0.001$). We next examined short-term regulation of neurotransmitter release by conducting paired-pulse recordings in 0.2 mM Ca^{2+} and discovered a significant increase in the paired-pulse ratio in *gyr* mutants (Fig. 9*D*; control = 1.5 ± 0.1, $n = 5$; *gyr* = 2.2 ± 0.2, $n = 6$; $p < 0.001$), consistent with a reduction in release probability in *gyr* mutants. Although *gyr* larvae exhibit an increase in paired-pulse facilitation, this enhanced facilitation is transient when examined using a longer stimulation protocol of 1500 stimuli at 20 Hz. After ~500 stimuli, the elevated facilitation in *gyr* larvae peaks and subsequently declines (Fig. 9*E*,*F*), indicating *gyr* synapses cannot maintain elevated levels of release and become depleted. We then sought to examine whether the delay in synaptic vesicle biogenesis from endocytic cisternae at *gyr* synapses translated into a defect in more long-term forms of synaptic plasticity induced by a brief 20 Hz stimulation in 2 mM Ca^{2+}. While *gyr* and control synapses exhibit a similar level of depression, the kinetics of recovery is slowed in *gyr* larvae as they have a more persistent post-tetanic depression (Fig. 9*G*), suggesting a defect in the replenishment of releasable vesicles. Although it is currently unclear how the loss of synaptogyrin precisely elicits changes in release properties, the defect in synaptic vesicle recycling and vesicle biogenesis may extend beyond regulating synaptic vesicle size to influencing synaptic vesicle protein content. An alteration in the normal distribution of synaptic vesicle proteins per vesicle could contribute to the abnormal release properties and synaptic plasticity in *gyr* mutants.

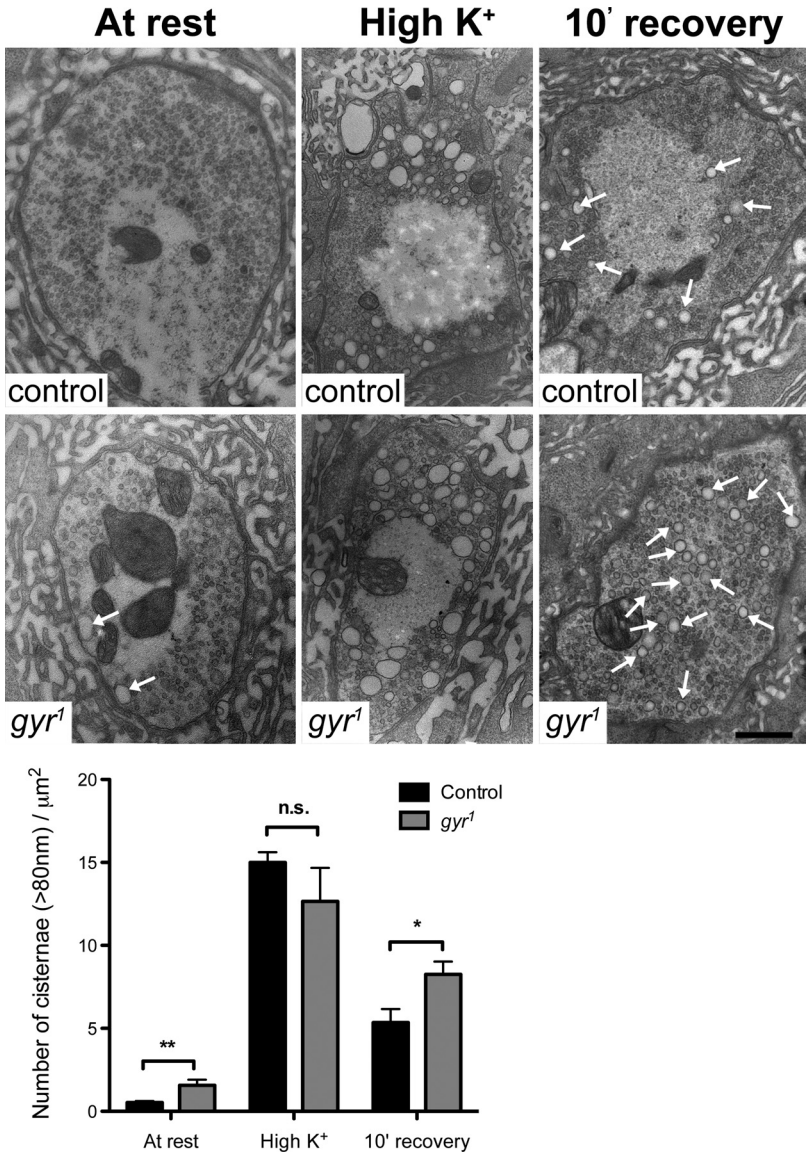

Figure 6. *gyr* mutants are delayed in resolving endocytic cisternae following a high K^+ saline shock. Left, At rest, *gyr* mutants have a statistically significant increase in the number of cisternae (endosomal-like structures larger than 80 nm in diameter) per μm^2 compared with controls ($p < 0.01$). Middle, Immediately following a 5 min incubation with high K^+ (90 mM) Jan and Jan solution, control and *gyr* boutons have a similar dramatic increase in the number of endocytic cisternae due to bulk endocytosis ($p = 0.21$). Right, Ten minutes after high K^+ stimulation, *gyr* boutons have ~50% more endocytic cisternae than controls, suggesting that they cannot resolve endocytic cisternae into synaptic vesicles as quickly as controls ($p = 0.01$). Arrows highlight cisternal structures. Scale bar, 500 nm.

Discussion

Synaptogyrin is not essential for synaptic vesicle trafficking

Our results indicate that synaptogyrin, while not essential for basal synaptic transmission in *Drosophila*, modulates synaptic vesicle cycling and impacts neurotransmitter release properties. Our findings are consistent with knock-out studies in other species that have identified relatively mild alterations in synaptic activity and vesicle morphology due to the loss of synaptogyrin and/or synaptophysin (McMahon et al., 1996; Janz et al., 1999; Abraham et al., 2006, 2011). While synaptogyrin and synaptophysin are not required for the generation of synaptic vesicles per se, increasing evidence suggests that these proteins play a facilitatory role in vesicle biogenesis and/or endocytosis. The *C. elegans* synaptogyrin/synaptophysin/SCAMP triple knock-out displayed an increase in clathrin-coated vesicles, which may reflect a compensatory mechanism for defects in other endocytic pathways (Abraham et al., 2006). Furthermore, the phenotypic severity of the endocytic mutants *endophilin*, *synaptotagmin*, and *synaptojanin* was enhanced when combined with mutations in *synaptogyrin* (Abraham et al., 2006, 2011). Murine retinal cells lacking both synaptophysin and its paralog synaptoporin had a decrease in synaptic vesicle density, and this reduction became more pronounced during periods of high activity (i.e., during dark adaptation). Moreover, during these periods of elevated activity there was an increase in the number of large cisternal-like structures, as well as an increase in synaptic vesicle diameter in synaptophysin knock-outs (Spiwoks-Becker et al., 2001). These results indicate that synaptophysin pro-

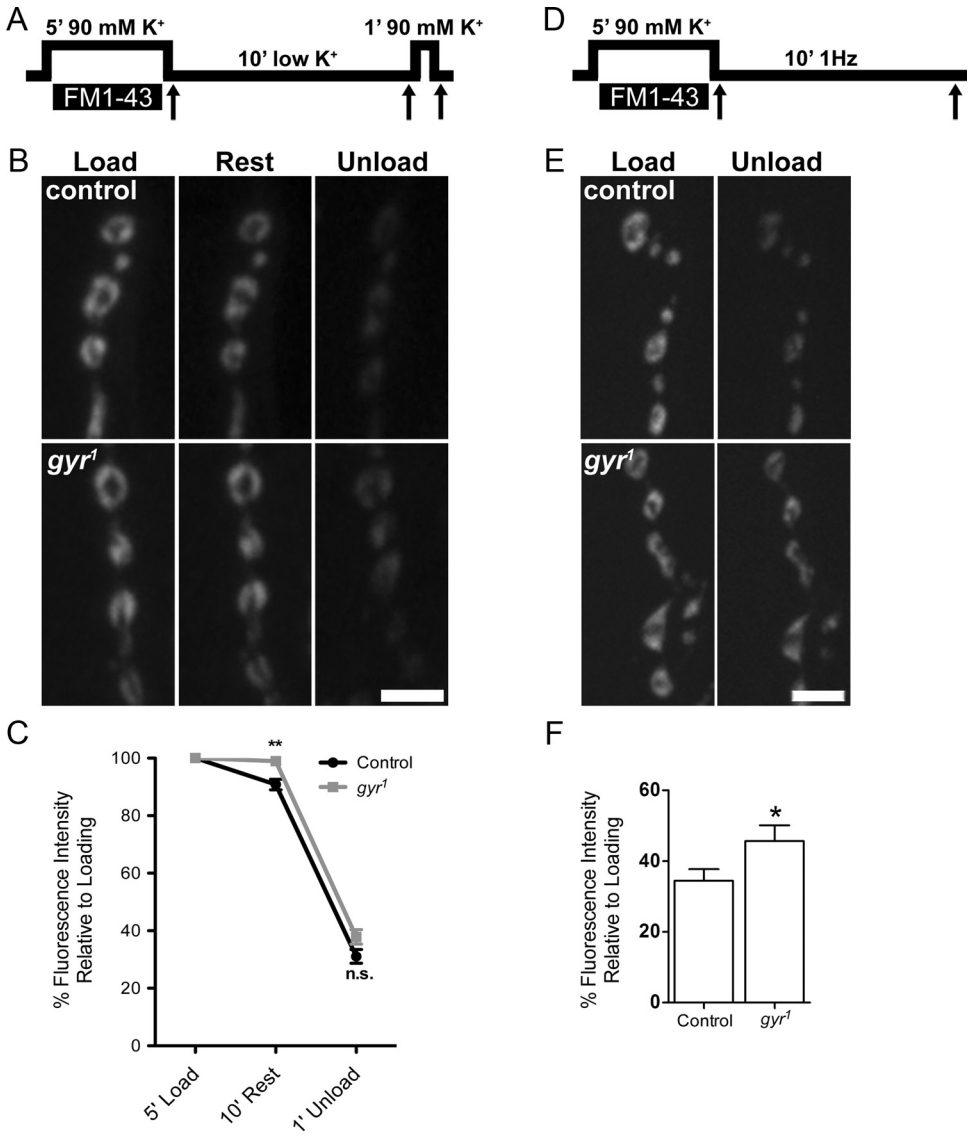

Figure 7. FM1–43 loading and unloading in *gyr* mutants. ***A***, Schematic of the FM1–43 loading/unloading protocol. Arrows indicate points at which images were acquired. ***B***, Representative images of control and *gyr* boutons from FM1–43 uptake experiments following 5 min of dye loading, 10 minutes of rest, and 1 min of dye unloading. Mean loading fluorescence intensity was not significantly different in *gyr* or control boutons. ***C***, Unloading fluorescence intensity relative to loading intensity was also unchanged in *gyr* mutants. Following a 10 min incubation in low K^+ saline, *gyr* boutons retained a statistically significant higher in fluorescence intensity relative to controls (control = 90.1 ± 1.83% relative to loading fluorescence, $n = 13$ NMJs; *gyr* = 98.9 ± 1.48%, $n = 11$ NMJs, $p < 0.01$). ***D***, Schematic of the FM1–43 loading/unloading protocol. ***E***, Representative images of control and *gyr* boutons after FM1–43 loading and 1 Hz frequency-induced unloading. ***F***, A significantly higher level of fluorescence intensity is retained in *gyr* boutons compared with control preparations following 1 Hz frequency-induced unloading (control = 34.5 ± 3.28% relative to loading fluorescence, $n = 19$ NMJs; *gyr* = 45.6 ± 4.47% $n = 18$ NMJs, $p < 0.05$). Scale bars: 5 μm.

motes the efficient formation of synaptic vesicles and that increased activity exacerbates this defect. Similarly, cultures derived from *synaptophysin* knock-out mice were slower to internalize tagged synaptic vesicle proteins during sustained stimulation, but not under mild stimulation conditions (Kwon and Chapman, 2011). These neurons also exhibited increased synaptic depression and delayed recovery of the synaptic vesicle pool, indicating that synaptophysin facilitates vesicle recovery. Our work suggests that synaptogyrin also modulates synaptic vesicle biogenesis in *Drosophila*, a species that lacks a synaptophysin homolog. The phenotypic variation we see at *gyr* boutons under resting conditions (Fig. 5) may reflect a difference in the levels of prior activity between boutons, which has previously been documented at *Drosophila* NMJs (Guerrero et al., 2005; Peled and Isacoff, 2011). Similar variability in phenotypic severity was observed in mammalian synaptojanin and dynamin 1 knock-out cultures, in which only a minority of synapses (predominantly GABAergic interneurons) displayed a dramatic accumulation of clathrin-coated pits, likely due to increased activity in these neurons (Hayashi et al., 2008).

Functional redundancy between synaptogyrin and synaptophysin has been demonstrated in mice (Janz et al., 1999). Therefore it is possible that the lack of strong phenotypes in flies, mice, and nematodes is due to compensation by a yet unidentified protein(s). SCAMPs, although lacking a MARVEL domain, have historically been linked with physins and gyrins because they share the same transmembrane topology and some SCAMP paralogs are located on synaptic vesicles (Brand et al., 1991; Fernández-Chacón and Südhof, 2000; Hübner et al., 2002). However, the lack of severe phenotypes in the *C. elegans* synaptogyrin/synaptophysin/SCAMP triple knock-out demonstrates that the absence of all of these protein families does not further impact basal synaptic function (Abraham et al., 2006). *Drosophila* has a

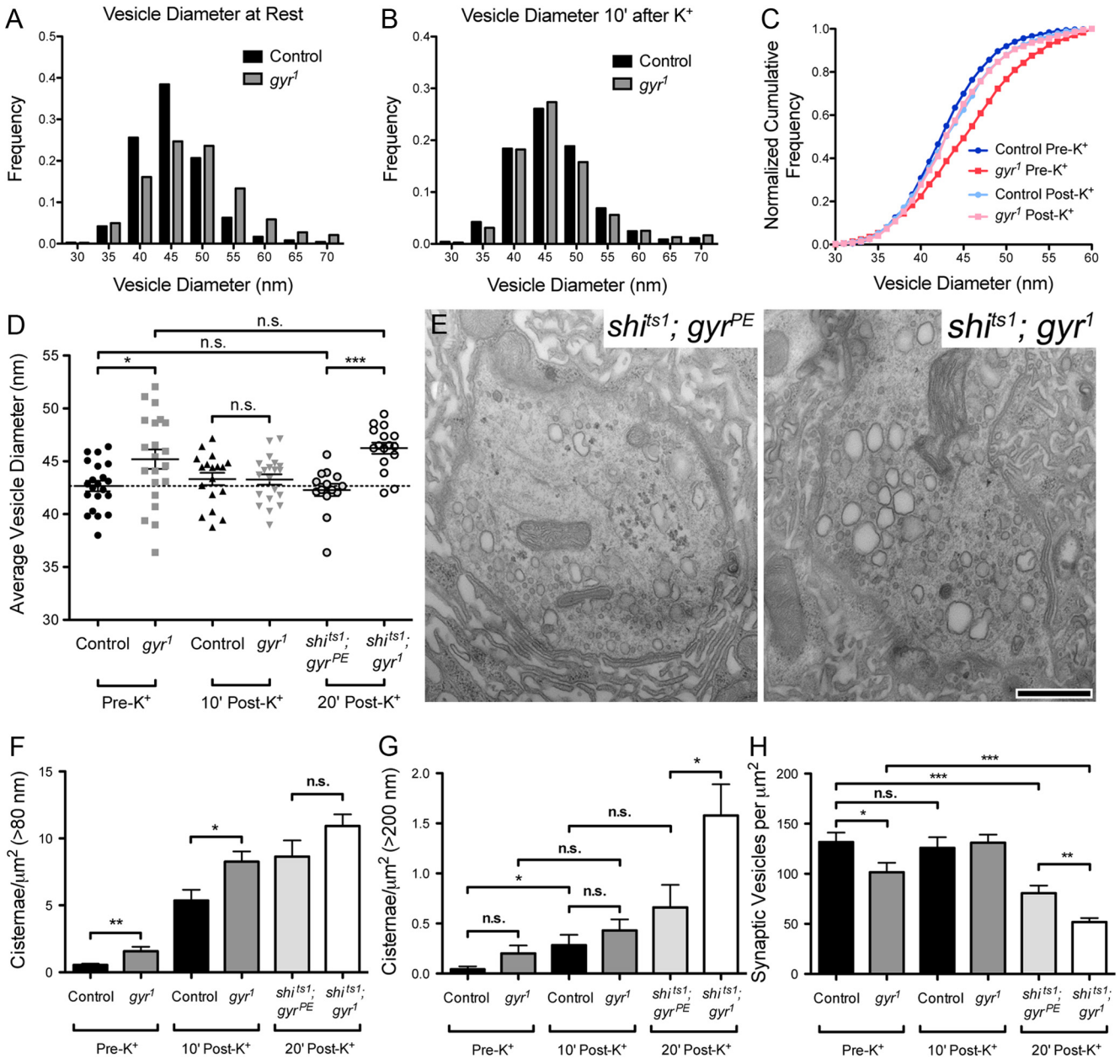

Figure 8. Effects of high K^+ stimulation on synaptic vesicle diameter and synaptic vesicle density. ***A***, Same as Figure 5*I*. At rest, *gyr* synaptic vesicles are larger and more variable in size. ***B***, Following a 5 min high K^+ shock and 10 min rest period, the distribution of synaptic vesicle diameter in *gyr* mutants is much more similar to controls. The mean synaptic vesicle diameter following the K^+ shock is not significantly different in *gyr* mutants relative to controls (control = 43.3 ± 0.58 nm, $n = 18$; *gyr* = 43.3 ± 0.50 nm, $n = 20$; $p = 0.95$). ***C***, A normalized cumulative frequency diagram illustrates the differences in vesicle diameter before (Pre-K^+) and after (Post-K^+) stimulation. Before the K^+ shock, the *gyr* distribution is slightly shifted to the right compared with the control. Following the K^+ shock, *gyr* and control synaptic vesicles have much more similar distributions. ***D***, The mean synaptic vesicle diameter of *gyr* boutons returns to control values following high K^+ stimulation. However, synaptic vesicle diameter in shi^{ts1}; gyr^1 larvae is significantly greater than shi^{ts1}; gyr^{PE} (shi^{ts1}; gyr^{PE} = 42.3 ± 0.58 nm, $n = 14$; shi^{ts1}; gyr^1 = 46.2 ± 0.52 nm, $n = 16$; $p < 0.001$). ***E***, Representative images of shi^{ts1}; gyr^{PE} and shi^{ts1}; gyr^1 boutons 20 min after a 5 min heat shock and high K^+ stimulation. ***F***, shi^{ts1}; gyr^{PE} and shi^{ts1}; gyr^1 have an increase in endocytic cisternae >80 nm in diameter after 20 min of recovery. ***G***, shi^{ts1}; gyr^1 boutons have a dramatic increase in the number of cisternae >200 nm in diameter ($p < 0.05$). Average number of cisternae >200 nm/μm^2 ± SEM: control (pre-K^+) = 0.042 ± 0.03, $n = 21$; gyr^1 (pre-K^+) = 0.20 ± 0.08, $n = 23$; control (post-K^+) = 0.28 ± 0.10, $n = 21$; gyr^1 (post-K^+) = 0.43 ± 0.11, $n = 22$; shi^{ts1}; gyr^{PE} (post-K^+) = 0.66 ± 0.22, $n = 14$; shi^{ts1}; gyr^1 (post-K^+) = 1.58 ± 0.31, $n = 17$). ***H***, Control and *gyr* boutons have similar synaptic vesicle densities after a high K^+ shock, while the presence of the *shibire* mutation results in a significant decrease in synaptic vesicle density following synaptic vesicle depletion, with shi^{ts1}; gyr^1 boutons displaying significantly lower levels than shi^{ts1}; gyr^{PE} ($p < 0.01$).

single SCAMP homolog, and is therefore amenable to further genetic analysis to examine issues of redundancy at fly synapses.

A model to explain synaptogyrin's role in synaptic vesicle formation

While there are still questions about synaptogyrin function, we propose a preliminary model to account for the *gyr* phenotypes related to abnormal synaptic vesicle diameter and delayed synaptic vesicle biogenesis from endocytic cisternae. Numerous studies have established the existence of multiple endocytic pathways at the NMJ, including clathrin-mediated and bulk endocytosis, as well as the controversial kiss-and-run pathway (Koenig and Ikeda, 1996; Verstreken et al., 2002; Dickman et al., 2005). We propose there are at least two pathways responsible for budding of synaptic vesicles from endocytic cisternae, one of which is regulated by synaptogyrin and the other that is independent of

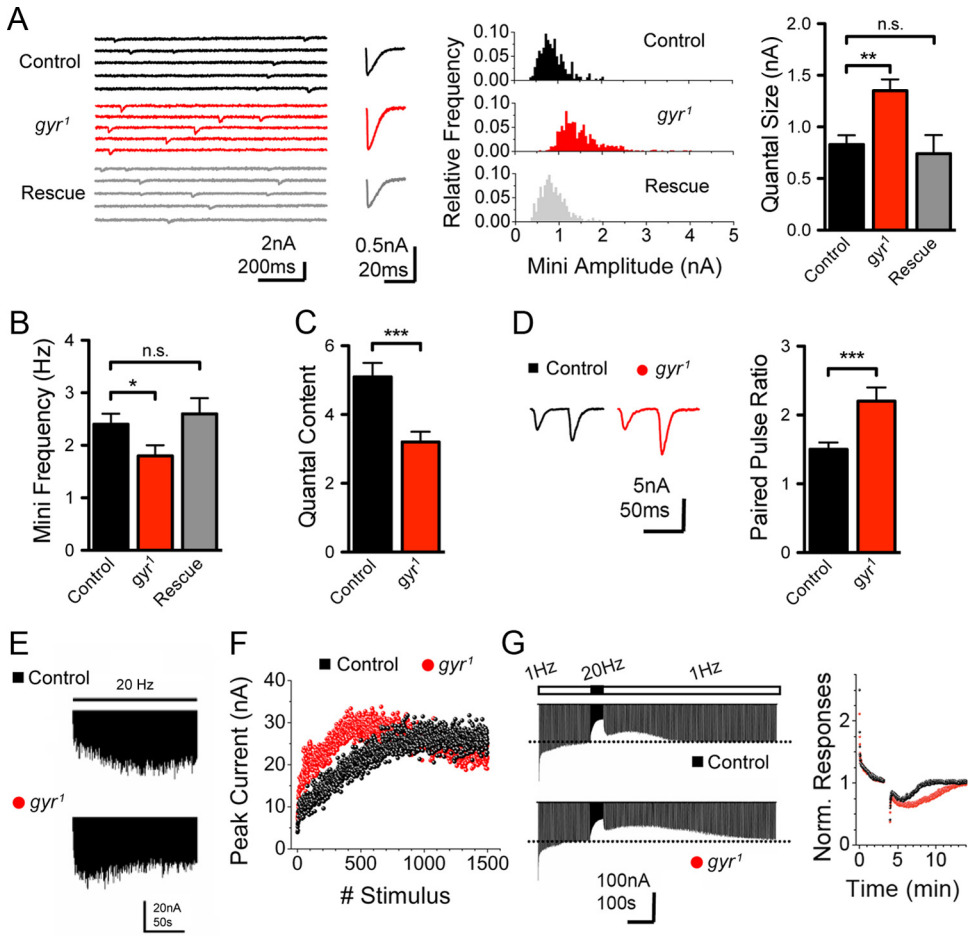

Figure 9. Electrophysiological analysis of *gyr* mutants. ***A***, Postsynaptic current recordings of spontaneous release at muscle 6 synapses in control (black), *gyr* (red), and rescue (gray) larvae. This genotypic color code is maintained throughout the figure. Histograms of mEJC peak amplitudes reveal a shift in the distribution toward higher values in *gyr* larvae, resulting in a significant increase in average mEJC amplitude ($p < 0.01$). Presynaptic expression of synaptogyrin driven by *elav*^{c155}*-GAL4* rescues the phenotypes. ***B***, Mini frequency is significantly decreased in *gyr* larvae ($p < 0.05$). ***C***, There is no significant change in evoked EJC amplitude ($p > 0.05$), while quantal content is reduced from 5.1 ± 0.4 quanta in controls to 3.2 ± 0.3 quanta in *gyr* ($p < 0.01$). ***D***, At 0.2 mM Ca^{2+}, *gyr* mutants have an increase in the paired-pulse ratio (PPR) compared with controls ($p < 0.001$). The PPR is defined as the amplitude of the second peak divided by the first peak. ***E***, Representative EJCs in low external Ca^{2+} (0.2 mM) in control and *gyr* synapses during a long 20 Hz tetanic stimulation. After an initial increase in facilitation, *gyr* larvae fail to maintain the increased EJC amplitude. ***F***, EJC amplitude change during a 20 Hz tetanic stimulation in control (black) and g*yr* (red) synapses. ***G***, Control and *gyr* synapses were stimulated at 1 Hz for 3 min to induce a low-frequency synaptic depression. This was followed by a 20 Hz stimulation train for 50 s in 2 mM Ca^{2+} to induce post-tetanic depression. Post-tetanic responses were then monitored at 1 Hz to examine synaptic recovery. *gyr* larvae require a significantly longer time to reach stable pre-tetanus EJC values following post-tetanic depression (5.1 ± 0.7 min in controls; 10.0 ± 1.3 min in *gyr*; $p < 0.01$). Normalized responses are plotted in the graph.

synaptogyrin function. In a wild-type bouton, both pathways are intact and produce vesicles of normal size, resulting in a low level of abnormal synaptic vesicles or residual endocytic cisternae. In the absence of synaptogyrin, the synaptogyrin-dependent pathway no longer functions properly and produces vesicles of abnormal size, while the synaptogyrin-independent pathway is still capable of generating normal synaptic vesicles. Nevertheless, the loss of synaptogyrin results in an overall increase in synaptic vesicle diameter in *gyr* animals.

During periods of intense activity that induce bulk endocytosis, a wild-type synapse has both pathways fully capable of regenerating synaptic vesicles from endocytic cisternae, and these structures quickly resolve into vesicles. However, in the *gyr* mutant, the synaptogyrin-dependent pathway is impaired, and the time it takes to resolve cisternae into synaptic vesicles is increased relative to controls. Furthermore, if the synaptogyrin-independent pathway is dominant in the *gyr* mutant, the synaptic vesicles that form shortly after intense stimulation would be more uniform in size because the vast majority would have been generated through the unimpaired synaptogyrin-independent pathway or via clathrin-mediated endocytosis from the plasma membrane.

An alternative model to the multiple endocytic pathways described above is that a single major endocytic pathway is responsible for vesicle biogenesis from cisternae, and the loss of synaptogyrin merely slows the process of synaptic vesicle budding. If synaptogyrin were involved in the budding of all synaptic vesicles from endocytic cisternae, one would expect to see a population of abnormally shaped synaptic vesicles shortly after the high K^+ shock as the cisternae begin to resolve, which we did not observe. However, it is unknown what fraction of vesicles generated after the K^+ shock originate directly from the plasma membrane as opposed to cisternae. If the majority of synaptic vesicles observed 10 min after high K^+ stimulation derive from the plasma membrane and this form of endocytosis is independent of synaptogyrin, then plasma membrane-derived synaptic vesicles may mask a small population of abnormal synaptic vesicles originating from cisternae in the *gyr* mutant. Indeed, the observation that synaptic vesicle diameter is increased and synaptic vesicle density is decreased in *shi*^{ts1}; *gyr*^{1} larvae following high K^+ stim-

ulation is consistent with this model. Assuming that dynamin inhibition forces a greater amount of synaptic membrane to cycle through endocytic cisternae, boutons lacking synaptogyrin would exhibit increased phenotypic severity. It should be noted, however, that the extent to which synaptogyrin influences traditional clathrin-mediated endocytosis from the plasma membrane is currently unknown.

Synaptogyrin regulates neurotransmitter release and short-term synaptic plasticity

Synaptic vesicle biogenesis, whether from an endosomal compartment or the plasma membrane, requires the recruitment of a wide variety of essential synaptic vesicle proteins. Maintaining the correct complement of synaptic vesicle proteins could theoretically be achieved through a kiss-and-run endocytic mechanism, which would allow a transiently fused vesicle to directly reform after fusion pore closure rather than collapse into the plasma membrane. While rapid endocytosis has been observed at certain synapses such as the calyx of Held (Wu et al., 2005), the contribution of kiss-and-run endocytosis at other synapses, including the *Drosophila* NMJ, is controversial (He and Wu, 2007). An alternative way to promote proper synaptic vesicle sorting would be through the creation of microdomains on the plasma membrane and endosomal cisternae enriched in the lipids and proteins found on individual synaptic vesicles. Synaptophysin, via its interactions with cholesterol and synaptobrevin, as well as its ability to multimerize, is an intriguing candidate to seed this sort of microdomain (Rehm et al., 1986; Thomas et al., 1988; Calakos and Scheller, 1994; Washbourne et al., 1995; Thiele et al., 2000).

If synaptogyrin influences the recruitment of synaptic vesicle proteins through the formation of membrane microdomains during endocytosis, the loss of synaptogyrin could lead to alterations in protein stoichiometry or protein sorting, which could impact synaptic vesicle release. Indeed, there is precedent for protein-sorting defects resulting in changes in exocytosis. A recent study investigating the function of a neuronal Rab35 GTPase activating protein named Skywalker (Sky) discovered that *sky* mutant larvae accumulate an excess of cisternal-like structures after intense stimulation and show increased neurotransmitter release relative to controls (Uytterhoeven et al., 2011). It remains to be determined whether the changes in neurotransmitter release observed in *gyr* mutants are the result of altered synaptic vesicle protein composition or whether synaptogyrin directly influences exocytosis through a currently unknown mechanism. Interestingly, several recent studies have associated mutations in the *synaptogyrin* locus with schizophrenia susceptibility in humans (Verma et al., 2004, 2005; Cheng and Chen, 2007; Iatropoulos et al., 2009). Therefore, defining how synaptogyrin controls synaptic vesicle cycling may provide insights into neuropsychiatric pathology.

References

Abraham C, Hutter H, Palfreyman MT, Spatkowski G, Weimer RM, Windoffer R, Jorgensen EM, Leube RE (2006) Synaptic tetraspan vesicle membrane proteins are conserved but not needed for synaptogenesis and neuronal function in Caenorhabditis elegans. Proc Natl Acad Sci U S A 103:8227–8232. CrossRef Medline

Abraham C, Bai L, Leube RE (2011) Synaptogyrin-dependent modulation of synaptic neurotransmission in Caenorhabditis elegans. Neuroscience 190:75–88. CrossRef Medline

Akbergenova Y, Bykhovskaia M (2009) Enhancement of the endosomal endocytic pathway increases quantal size. Mol Cell Neurosci 40:199–206. CrossRef Medline

Arthur CP, Stowell MH (2007) Structure of synaptophysin: a hexameric MARVEL-domain channel protein. Structure 15:707–714. CrossRef Medline

Barber CF, Jorquera RA, Melom JE, Littleton JT (2009) Postsynaptic regulation of synaptic plasticity by synaptotagmin 4 requires both C2 domains. J Cell Biol 187:295–310. CrossRef Medline

Belfort GM, Bakirtzi K, Kandror KV (2005) Cellugyrin induces biogenesis of synaptic-like microvesicles in PC12 cells. J Biol Chem 280:7262–7272. CrossRef Medline

Brand AH, Perrimon N (1993) Targeted gene expression as a means of altering cell fates and generating dominant phenotypes. Development 118:401–415. Medline

Brand SH, Laurie SM, Mixon MB, Castle JD (1991) Secretory carrier membrane proteins 31–35 define a common protein composition among secretory carrier membranes. J Biol Chem 266:18949–18957. Medline

Budnik V, Zhong Y, Wu CF (1990) Morphological plasticity of motor axons in *Drosophila* mutants with altered excitability. J Neurosci 10:3754–3768. Medline

Calakos N, Scheller RH (1994) Vesicle-associated membrane protein and synaptophysin are associated on the synaptic vesicle. J Biol Chem 269:24534–24537. Medline

Cheng MC, Chen CH (2007) Identification of rare mutations of synaptogyrin 1 gene in patients with schizophrenia. J Psychiatr Res 41:1027–1031. CrossRef Medline

Cho RW, Song Y, Littleton JT (2010) Comparative analysis of Drosophila and mammalian complexins as fusion clamps and facilitators of neurotransmitter release. Mol Cell Neurosci 45:389–397. CrossRef Medline

Cochilla AJ, Angleson JK, Betz WJ (1999) Monitoring secretory membrane with FM1–43 fluorescence. Annu Rev Neurosci 22:1–10. CrossRef Medline

Collins CA, DiAntonio A (2007) Synaptic development: insights from Drosophila. Curr Opin Neurobiol 17:35–42. CrossRef Medline

Daly C, Ziff EB (2002) Ca2+-dependent formation of a dynamin-synaptophysin complex: potential role in synaptic vesicle endocytosis. J Biol Chem 277:9010–9015. CrossRef Medline

Daly C, Sugimori M, Moreira JE, Ziff EB, Llinás R (2000) Synaptophysin regulates clathrin-independent endocytosis of synaptic vesicles. Proc Natl Acad Sci U S A 97:6120–6125. CrossRef Medline

De Camilli P, Takei K (1996) Molecular mechanisms in synaptic vesicle endocytosis and recycling. Neuron 16:481–486. CrossRef Medline

de Lange RP, de Roos AD, Borst JG (2003) Two modes of vesicle recycling in the rat calyx of Held. J Neurosci 23:10164–10173. Medline

Dickman DK, Horne JA, Meinertzhagen IA, Schwarz TL (2005) A slowed classical pathway rather than kiss-and-run mediates endocytosis at synapses lacking synaptojanin and endophilin. Cell 123:521–533. CrossRef Medline

Dickman DK, Lu Z, Meinertzhagen IA, Schwarz TL (2006) Altered synaptic development and active zone spacing in endocytosis mutants. Curr Biol 16:591–598. CrossRef Medline

Di Tommaso P, Moretti S, Xenarios I, Orobitg M, Montanyola A, Chang JM, Taly JF, Notredame C (2011) T-Coffee: a web server for the multiple sequence alignment of protein and RNA sequences using structural information and homology extension. Nucleic Acids Res 39:W13–W17. CrossRef Medline

Edelmann L, Hanson PI, Chapman ER, Jahn R (1995) Synaptobrevin binding to synaptophysin: a potential mechanism for controlling the exocytotic fusion machine. EMBO J 14:224–231. Medline

Estrada B, Maeland AD, Gisselbrecht SS, Bloor JW, Brown NH, Michelson AM (2007) The MARVEL domain protein, Singles Bar, is required for progression past the pre-fusion complex stage of myoblast fusion. Dev Biol 307:328–339. CrossRef Medline

Evans GJ, Cousin MA (2007) Activity-dependent control of slow synaptic vesicle endocytosis by cyclin-dependent kinase 5. J Neurosci 27:401–411. CrossRef Medline

Fernández-Chacón R, Südhof TC (2000) Novel SCAMPs lacking NPF repeats: ubiquitous and synaptic vesicle-specific forms implicate SCAMPs in multiple membrane-trafficking functions. J Neurosci 20:7941–7950. Medline

Furuse M, Tsukita S (2006) Claudins in occluding junctions of humans and flies. Trends Cell Biol 16:181–188. CrossRef Medline

Gincel D, Shoshan-Barmatz V (2002) The synaptic vesicle protein synapto-

physin: purification and characterization of its channel activity. Biophys J 83:3223–3229. CrossRef Medline

Granseth B, Odermatt B, Royle SJ, Lagnado L (2006) Clathrin-mediated endocytosis is the dominant mechanism of vesicle retrieval at hippocampal synapses. Neuron 51:773–786. CrossRef Medline

Guan Z, Saraswati S, Adolfsen B, Littleton JT (2005) Genome-wide transcriptional changes associated with enhanced activity in the Drosophila nervous system. Neuron 48:91–107. CrossRef Medline

Guerrero G, Rieff DF, Agarwal G, Ball RW, Borst A, Goodman CS, Isacoff EY (2005) Heterogeneity in synaptic transmission along a Drosophila larval motor axon. Nat Neurosci 8:1188–1196. CrossRef Medline

Hartline DK, Colman DR (2007) Rapid conduction and the evolution of giant axons and myelinated fibers. Curr Biol 17:R29–R35. CrossRef Medline

Hayashi M, Raimondi A, O'Toole E, Paradise S, Collesi C, Cremona O, Ferguson SM, De Camilli P (2008) Cell- and stimulus-dependent heterogeneity of synaptic vesicle endocytic recycling mechanisms revealed by studies of dynamin 1-null neurons. Proc Natl Acad Sci U S A 105:2175–2180. CrossRef Medline

He L, Wu LG (2007) The debate on the kiss-and-run fusion at synapses. Trends Neurosci 30:447–455. CrossRef Medline

Heuser JE, Reese TS (1973) Evidence for recycling of synaptic vesicle membrane during transmitter release at the frog neuromuscular junction. J Cell Biol 57:315–344. CrossRef Medline

Hubbard C, Singleton D, Rauch M, Jayasinghe S, Cafiso D, Castle D (2000) The secretory carrier membrane protein family: structure and membrane topology. Mol Biol Cell 11:2933–2947. Medline

Hübner K, Windoffer R, Hutter H, Leube RE (2002) Tetraspan vesicle membrane proteins: synthesis, subcellular localization, and functional properties. Int Rev Cytol 214:103–159. CrossRef Medline

Huntwork S, Littleton JT (2007) A complexin fusion clamp regulates spontaneous neurotransmitter release and synaptic growth. Nat Neurosci 10:1235–1237. CrossRef Medline

Iatropoulos P, Gardella R, Valsecchi P, Magri C, Ratti C, Podavini D, Rossi G, Gennarelli M, Sacchetti E, Barlati S (2009) Association study and mutational screening of SYNGR1 as a candidate susceptibility gene for schizophrenia. Psychiatr Genet 19:237–243. CrossRef Medline

Jan LY, Jan YN (1976) L-glutamate as an excitatory transmitter at the Drosophila larval neuromuscular junction. J Physiol 262:215–236. Medline

Janz R, Südhof TC, Hammer RE, Unni V, Siegelbaum SA, Bolshakov VY (1999) Essential roles in synaptic plasticity for synaptogyrin I and synaptophysin I. Neuron 24:687–700. CrossRef Medline

Kay AR, Alfonso A, Alford S, Cline HT, Holgado AM, Sakmann B, Snitsarev VA, Stricker TP, Takahashi M, Wu LG (1999) Imaging synaptic activity in intact brain and slices with FM1–43 in C. elegans, lamprey, and rat. Neuron 24:809–817. CrossRef Medline

Khodosh R, Augsburger A, Schwarz TL, Garrity PA (2006) Bchs, a BEACH domain protein, antagonizes Rab11 in synapse morphogenesis and other developmental events. Development 133:4655–4665. CrossRef Medline

King N, et al. (2008) The genome of the choanoflagellate Monosiga brevicollis and the origin of metazoans. Nature 451:783–788. CrossRef Medline

Koenig JH, Ikeda K (1996) Synaptic vesicles have two distinct recycling pathways. J Cell Biol 135:797–808. CrossRef Medline

Koh TW, Verstreken P, Bellen HJ (2004) Dap160/intersectin acts as a stabilizing scaffold required for synaptic development and vesicle endocytosis. Neuron 43:193–205. CrossRef Medline

Koh TW, Korolchuk VI, Wairkar YP, Jiao W, Evergren E, Pan H, Zhou Y, Venken KJ, Shupliakov O, Robinson IM, O'Kane CJ, Bellen HJ (2007) Eps15 and Dap160 control synaptic vesicle membrane retrieval and synapse development. J Cell Biol 178:309–322. CrossRef Medline

Kwon SE, Chapman ER (2011) Synaptophysin regulates the kinetics of synaptic vesicle endocytosis in central neurons. Neuron 70:847–854. CrossRef Medline

Lnenicka GA, Keshishian H (2000) Identified motor terminals in Drosophila larvae show distinct differences in morphology and physiology. J Neurobiol 43:186–197. CrossRef Medline

Markstein M, Pitsouli C, Villalta C, Celniker SE, Perrimon N (2008) Exploiting position effects and the gypsy retrovirus insulator to engineer precisely expressed transgenes. Nat Genet 40:476–483. CrossRef Medline

Marxen M, Volknandt W, Zimmermann H (1999) Endocytic vacuoles formed following a short pulse of K+-stimulation contain a plethora of presynaptic membrane proteins. Neuroscience 94:985–996. CrossRef Medline

McMahon HT, Bolshakov VY, Janz R, Hammer RE, Siegelbaum SA, Südhof TC (1996) Synaptophysin, a major synaptic vesicle protein, is not essential for neurotransmitter release. Proc Natl Acad Sci U S A 93:4760–4764. CrossRef Medline

Miller TM, Heuser JE (1984) Endocytosis of synaptic vesicle membrane at the frog neuromuscular junction. J Cell Biol 98:685–698. CrossRef Medline

Ni JQ, Markstein M, Binari R, Pfeiffer B, Liu LP, Villalta C, Booker M, Perkins L, Perrimon N (2008) Vector and parameters for targeted transgenic RNA interference in Drosophila melanogaster. Nat Methods 5:49–51. CrossRef Medline

Nonet ML (1999) Visualization of synaptic specializations in live C. elegans with synaptic vesicle protein-GFP fusions. J Neurosci Methods 89:33–40. CrossRef Medline

Notredame C, Higgins DG, Heringa J (2000) T-Coffee: a novel method for fast and accurate multiple sequence alignment. J Mol Biol 302:205–217. CrossRef Medline

Peled ES, Isacoff EY (2011) Optical quantal analysis of synaptic transmission in wild-type and rab3-mutant Drosophila motor axons. Nat Neurosci 14:519–526. CrossRef Medline

Plate M, Li T, Wang Y, Mo X, Zhang Y, Ma D, Han W (2010) Identification and characterization of CMTM4, a novel gene with inhibitory effects on HeLa cell growth through Inducing G2/M phase accumulation. Mol Cells 29:355–361. CrossRef Medline

Putnam NH, Srivastava M, Hellsten U, Dirks B, Chapman J, Salamov A, Terry A, Shapiro H, Lindquist E, Kapitonov VV, Jurka J, Genikhovich G, Grigoriev IV, Lucas SM, Steele RE, Finnerty JR, Technau U, Martindale MQ, Rokhsar DS (2007) Sea anemone genome reveals ancestral eumetazoan gene repertoire and genomic organization. Science 317:86–94. CrossRef Medline

Rehm H, Wiedenmann B, Betz H (1986) Molecular characterization of synaptophysin, a major calcium-binding protein of the synaptic vesicle membrane. EMBO J 5:535–541. Medline

Richards DA, Guatimosim C, Betz WJ (2000) Two endocytic recycling routes selectively fill two vesicle pools in frog motor nerve terminals. Neuron 27:551–559. CrossRef Medline

Richards DA, Guatimosim C, Rizzoli SO, Betz WJ (2003) Synaptic vesicle pools at the frog neuromuscular junction. Neuron 39:529–541. CrossRef Medline

Sánchez-Pulido L, Martín-Belmonte F, Valencia A, Alonso MA (2002) MARVEL: a conserved domain involved in membrane apposition events. Trends Biochem Sci 27:599–601. CrossRef Medline

Spiwoks-Becker I, Vollrath L, Seeliger MW, Jaissle G, Eshkind LG, Leube RE (2001) Synaptic vesicle alterations in rod photoreceptors of synaptophysin-deficient mice. Neuroscience 107:127–142. CrossRef Medline

Srivastava M, et al. (2008) The Trichoplax genome and the nature of placozoans. Nature 454:955–960. CrossRef Medline

Srivastava M, et al. (2010) The Amphimedon queenslandica genome and the evolution of animal complexity. Nature 466:720–726. CrossRef Medline

Takamori S, et al. (2006) Molecular anatomy of a trafficking organelle. Cell 127:831–846. CrossRef Medline

Takei K, Mundigl O, Daniell L, De Camilli P (1996) The synaptic vesicle cycle: a single vesicle budding step involving clathrin and dynamin. J Cell Biol 133:1237–1250. CrossRef Medline

Thiele C, Hannah MJ, Fahrenholz F, Huttner WB (2000) Cholesterol binds to synaptophysin and is required for biogenesis of synaptic vesicles. Nat Cell Biol 2:42–49. CrossRef Medline

Thomas L, Hartung K, Langosch D, Rehm H, Bamberg E, Franke WW, Betz H (1988) Identification of synaptophysin as a hexameric channel protein of the synaptic vesicle membrane. Science 242:1050–1053. CrossRef Medline

Uytterhoeven V, Kuenen S, Kasprowicz J, Miskiewicz K, Verstreken P (2011) Loss of skywalker reveals synaptic endosomes as sorting stations for synaptic vesicle proteins. Cell 145:117–132. CrossRef Medline

Verma R, Chauhan C, Saleem Q, Gandhi C, Jain S, Brahmachari SK (2004) A nonsense mutation in the synaptogyrin 1 gene in a family with schizophrenia. Biol Psychiatry 55:196–199. CrossRef Medline

Verma R, Kubendran S, Das SK, Jain S, Brahmachari SK (2005) SYNGR1 is

associated with schizophrenia and bipolar disorder in southern India. J Hum Genet 50:635–640. CrossRef Medline

Verstreken P, Kjaerulff O, Lloyd TE, Atkinson R, Zhou Y, Meinertzhagen IA, Bellen HJ (2002) Endophilin mutations block clathrin-mediated endocytosis but not neurotransmitter release. Cell 109:101–112. CrossRef Medline

Verstreken P, Koh TW, Schulze KL, Zhai RG, Hiesinger PR, Zhou Y, Mehta SQ, Cao Y, Roos J, Bellen HJ (2003) Synaptojanin is recruited by endophilin to promote synaptic vesicle uncoating. Neuron 40:733–748. CrossRef Medline

Wagh DA, Rasse TM, Asan E, Hofbauer A, Schwenkert I, Dürrbeck H, Buchner S, Dabauvalle MC, Schmidt M, Qin G, Wichmann C, Kittel R, Sigrist SJ, Buchner E (2006) Bruchpilot, a protein with homology to ELKS/CAST, is required for structural integrity and function of synaptic active zones in Drosophila. Neuron 49:833–844. CrossRef Medline

Washbourne P, Schiavo G, Montecucco C (1995) Vesicle-associated membrane protein-2 (synaptobrevin-2) forms a complex with synaptophysin. Biochem J 305:721–724. Medline

Wu W, Xu J, Wu XS, Wu LG (2005) Activity-dependent acceleration of endocytosis at a central synapse. J Neurosci 25:11676–11683. CrossRef Medline